SNO-STR-91-06

Extraction of Data in SNO for various MSW Scenarios

P. Skensved and B.C. Robertson
SNO-STR-91-06

20-Feb-1991

Introduction

The response of the SNO detector has been investigated for three different Δm^2, $\sin^2 2\theta$ scenarios and for the case of vacuum oscillations. In each case spectra simulating a light water fill, a heavy water fill and finally a heavy water plus NaCl fill were generated. Each counting period was taken to be one year. The three neutrino oscillation cases were chosen somewhat arbitrarily as the midpoints of each of the three legs of the familiar MSW triangle. The ν_e spectra were taken from [1].

The response to both internal and external backgrounds were simulated and added to give a total 3 year 'observed' data set. These sets were sorted with respect to energy, angle and reconstructed radius. Attempts were made to extract the ν_e and ν_x components.

Calculations

In its present form, the SNO detector consists of 1,000 tonnes of D_2O contained in a 2" thick spherical acrylic vessel with a radius of 600 cm, viewed by 9,500 Hamamatsu 8" R1408 phototubes. A reflector with a 56 degree cut-off angle is mounted on each phototube and the front face of the reflector is positioned 2.5 meters from the D_2O. For these simulations we assume a phototube timing of 1.61 ns (σ) and we employ an elliptical approximation for the reflector shape. The reflector surface is assumed to be metallic Aluminum with a reflectivity of 92% at 400 nm.

The basic Monte-Carlo code has been described elsewhere [2, 3, 4]. It uses EGS4 to do the charged particle and γ-ray transport and code developed at Queen's for tracking the Čerenkov light. Event reconstruction is done with a simple point fitter which minimizes the transit time differences in an iterative fashion.

Backgrounds

There are 3 major background components. The first one is due to low energy β-γ cascades from the bottom of the ^{232}Th and ^{238}U chains. The second one comes from high energy (5 to 10 MeV) neutron capture γ-rays. These neutrons are created by α-particles from the ^{232}Th and ^{238}U chains via (α,n) reactions on light isotopes. Since the (α,n) cross sections are small, such backgrounds occur only in 'dirty' materials like the rock, concrete and steel in the cavity surroundings and in the PMT's and their support structure. Finally, the third type of backgrounds in SNO is neutrons created by photodisintegration in the D_2O. Any γ-ray with an energy above 2.2 MeV in the D_2O has a potential for generating a free neutron.

The amount of Th and U in the various detector components is listed in table 1. For the D_2O, Acrylic and H_2O the levels are the same as those used for the 'White Book' [5]. For the β-γ's in the phototubes the effective amount of Th and U was taken to be 100 ppb. This is higher than previously assumed by a factor of 2.5 . New measurements have indicated that there

is high activity ($\approx$ ppm) pin-out glass and ceramic spacers inside the PMT. The high energy background was derived from the results given in [6], where detailed calculations for each component are summarized.

Generation of data

The levels of Th are such that a full year can be simulated with the code within a reasonable time for the 'internal' components (inside 850 cm). Since the decay rate for Uranium is higher than that of Thorium, but the energy is lower, only $\frac{1}{10}$ of a year was simulated for it. For the PMT's the levels are too high to simulate more than a small fraction of one day ($\approx$ 4 hrs. for Th).

For these simulations the code was set up to save the fitted position, direction and number of hits for events which reconstructed inside 850 cm with 16 or more hits. Initial position and direction was also saved. The resulting files were scanned and sorted into 3-dimensional histograms (energy versus cosine of angle to the Sun versus number of counts) for various radial cuts. The angular side was divided into 40 bins between -1 and +1. By summing appropriate subsets of the M.C. data a complete 3 year (H_2O, D_2O and D_2O with NaCl) data set can be created. However, only one set of simulations was done for the β-γ's. Consequently correlations exists at low N_{hit} between the data sets but for the thresholds used in the analysis described below this is not a serious problem. At 40 hits, which is the minimum used, there is little contribution from the 'β-γ wall'.

Figure 1 shows the number of events reconstructed inside a radius of 600 cm for year 3 assuming vacuum oscillations and a total flux of 5.8 $\times$ 10^6 cm^2 s^{-1}. Equivalent plots for 700 cm and 500 cm are shown in figures 2 and 3.

Extraction of data

One of the first questions to be answered by SNO is : can we prove or reject the MSW hypothesis ? In the context of the present simulations the question can be rephrased : assuming we know the cross sections and assuming we know the response of the detector and given a 3 year data set, can we fit it to the no-oscillation hypothesis within 3σ ?

To answer this question additional high statistics (10 to 20 years) runs were done for an undistorted ^{8}B neutrino spectrum to get the ES, CC and NC 'parent' distributions. These were sorted the same way as the 'data' according to energy, angle and radius.

Initially, attempts were made to fit the energy-angle distributions (for fixed radial cut) to the data sets. These attempts were not successful in part due to the low statistics in each bin. Dividing a years worth of data into 200 $\times$ 40 bins produces many bins with zero counts. Reducing the number of bins does not make the situation much better. For the present detector the energy calibration is approximately 9.5 hits per MeV so that working with less than 50 bins in the energy side would not be reasonable (the energy range is 20 MeV). Twenty bins for the angle would compress the elastic scattering peak into less than 3 channels which is borderline for fitting the angular shape. Fifty by twenty still give us 1000 bins to divide the data over and even that leads to problems. Furthermore, we do not know the shape of the CC spectrum, the ES spectrum or the high energy background tail *a priori* [1] Allowing the neutrino spectrum shape to change introduces another two parameters into the fit.

A simpler (and more successful) approach is to use just the angular projections. The elastic scattering angular distribution is very insensitive to the energy threshold and to spectral distortions [7]. The CC reaction has a simple angular dependence independent of energy, $1 - Q_1 \times \frac{1}{3} \times \cos\theta$ where Q_1 (the smearing due to detector angular resolution) equals one to a very good approximation. Finally, the rest is isotropic. This includes the NC signal, the NC background and the high energy γ-ray background. Thus we can fit the data to ES(θ) + [$1 + \frac{1}{3}cos\theta$] + constant.

[1] The high energy tail is dealt with in a separate section.

To illustrate what is going on, one case (year 3, $\Delta m^2 = 10^{-6}$, $\sin^2 2\theta = .01$) will be looked at in more detail. Figure 4a shows the energy projection of the total (the 'observed' spectrum) for r $\leq$ 600 cm. The next seven figures (4b through 4h) shows the effect of varying the lower threshold between 30 and 70 hits on the angular projection. The elastic scattering peak is clearly visible at 40, slightly below the 'wall'. Above 70 hits it decreases rapidly. The optimum threshold is somewhere around 45 hits.

The fits to this data set for thresholds of 40, 50, 60 and 70 hits is shown in figures 5a through 5d. The quality is generally quite good. Year 1 and year 2 data look similar - we can analyze from about 40 to 70 hits. In year 1 the fit is to ES(θ) + constant only. Fits for a 50 hit threshold for all three years is shown in figure 6.

Fitting the data in the case of vacuum oscillations yield similar results (figure 7) and the same data is presented in numerical form in the tables 2 to 5 for each of the three years. Tables 2, 3 and 4 contains the numbers extracted, the numbers put into the Monte Carlo and the total table 5 lists the same numbers in ratio form.

The last two cases are shown in figures 8 and 9. In the case of no (or small) distortion what is put in can be extracted but if there are distortions we are unable to separate NC events from CC events. It is also clear from table 3 that year 2 gives us little useful information about the neutral current - it may in fact mislead us. There are large correlation coefficients in all the fits between the ES and the CC (typically 0.60) and between the CC and the NC components (typically -0.98). For ES - NC the value is around -0.65 .

Table 6 lists the expected rates based on the high statistics multi year spectra for the Standard Solar Model with a ν_e flux of 5.8×10^6 cm^2 s^{-1} and a radial cut of 600 cm.

If we normalize the numbers in table 4 to the expected ones for no oscillations (table 6) we get table 7. Again, it is clear that there is no real measurement of the ν_x flux in year 2 . The numbers are in agreement with what one would expect. For the case $\Delta m^2 = 10^{-6}$ (suppression of low energy ν_e's) we just see an overall reduction relative to the undistorted case.

The same is the case for 10^{-5} where the ν_e flux is uniformly suppressed. In the last case (10^{-4}) the extracted flux divide by the expected one decreases as function of energy consistent with suppression of high energy ν_e's.

ν_x/ν_e flux

Given numbers like those in tables 2, 3 and 4 we can extract the ν_x/ν_e flux ratio by forming the ratio :

$$R = [NC_{obs}/CC_{obs}] \times [CC_{mc}/NC_{mc}]$$

where the CC_{mc} and NC_{mc} are evaluated for the no oscillation case. Several assumptions are involved here. We have to assume that the Monte Carlo code gives us the correct ratio between Neutral Current and Charged Current above whatever threshold we are using. Also, the cross section ratio must be known accurately. Calculations [8] with different nucleon-nucleon potentials indicate that the cross section ratio is determined to better than 5% for for neutrino energies above 5 MeV. Below that the calculations deviate significantly from each other.

The ratio R will be larger than one since NC_{obs} contains a background component. However, if the extracted ratio after correction for background is sufficiently different from one and the uncertainty is low enough then we can conclude that oscillations definitely exists.

There are two components in the neutron background; the 'internal' one from the D_2O (which looks like the signal) and the 'external' from the Acrylic and sources beyond. Since the energy calibration is rather flat as function of radius in the D_2O there is little difference in the response between an 'internal' and an 'external' neutron. What matters is therefore just the *total* number of neutrons captured from various components. This also means that the extracted ratio can be corrected by a simple factor of form $[1 + \frac{B}{S}]$ where B is the the number of 'background' neutrons and S is the number of 'signal' neutrons.

In the following we will assume that the absolute amounts of Th and U can be determined to 20% or better by independent measurements of

both the Acrylic and the D_2O. [2] The total number of neutrons generated can be calculated and from a neutron transport calculation the number of captures and their positions can be determined. Based on radioactivities and masses from table 1 there are a total of 1792 captures in year 3 of which 1191 come from the D_2O. This is what is put into the generated spectra.

Figure 10 shows the background corrected R for a threshold of 50 hits as function of the neutron background measured in units of 1792 capture neutrons per year. The interpretation of this plot is as follows : Suppose we measured the neutron background independently but underestimated it by a factor of two. Then in the case of $\Delta m^2 = 10^{-6}$ we would conclude that the data is inconsistent with the no-oscillation hypothesis to about 2σ. If, on the other hand, we overestimated the neutron background by a factor of 3 then we could not reject the no-oscillation hypothesis. For this plot we have used NC numbers from year 3 and CC numbers from year 2 in order to avoid contributions to the uncertainty from the correlations. Despite doing this, the uncertainties are still rather large making it impossible to reach any firm conclusions. A large part of the uncertainty comes from the lack of distinction between NC and CC events. Fitting the energy side as well would not necessarily improve the situation since as pointed out above we do not know the shape of 3 of the 4 components involved.

An alternative method which does not involve the uncertainties associated with fitting the data will however produce quite conclusive results. If our analysis threshold is sufficiently high so that we are above the tail of the 'internal' β-γ's then the remaining backgrounds (cavity and PMT support structure) is constant from year to year. Assuming then that the counting period are the same we can form the ratio $r = \frac{T_3 - T_2}{T_2 - T_1}$ where T_i refers to the total number of counts above the threshold in year i . This quantity is related to R via : $R = \frac{r}{1 - n - nXr}$ where n is the ratio of the relative neutron efficiencies in year 2 and year 3. For this report we calculate n from the high statistics runs. In real life it can be determined from source runs. The result is figure 11 which is a vast improvement over figure 10. If we get the neutron background more or less right there is no question (except perhaps in the case of $\Delta m^2 = 10^{-6}$) that oscillations are present. Extracting the values of Δm^2 and $\sin^2 2\theta$ would of course depend critically

[2] The question of whether or not we can extract the 'external' component from the data will be dealt with later.

on the amount of neutron background subtracted.

Analysis for smaller radii

The only reason to do analysis for smaller radii would be in case the external neutron background is too high to handle reliably. As far as the the Charged Current signal goes a factor of two increase in the radioactivity outside the D_2O would have little effect. The threshold would have to be increased by a few N_{hit} which would not change the extracted CC and ES numbers significantly. Therefore, the maximum analysis radius is defined by the size of the 'external' neutron component relative to the signal and the 'internal' components.

With the assumed 'external' neutron background level (based on table 1) the statistics gets worse as we go to smaller radius due to the loss of fiducial volume. Tables 8, 9 and 10 lists the numbers extracted for $\Delta m^2 = 10^{-6}$ with a radial cut of 500 cm. Figure 12 shows the fits for year 1,2 and 3 for a threshold of 50 hits. The expected numbers can be found in table 11 and the extracted to observed ratios are in table 12

Acrylic neutron background

In the analysis above we assumed that the 'external' neutron background (primarily the Acrylic) could be determined independently by other means. It is of interest to see whether we could extract it from the data itself. As an example we have picked the no-oscillation scenario and analyzed for the standard 'White Book' background ($\times$ 1) and one where the Acrylic is ten times more radioactive ($\times$ 10). The generated spectra were sorted according to radial bin and figure 13 shows the total number of events above 50 hits (divided by the volumes) as a function of radius. The divisions between the bins were : 200, 300, 400, 450, 500, 550 and 600 cm. The solid curve is the Monte Carlo prediction (based on the high statistics data). It includes everything except the external NC background. The deviation between it and the $\times$ 1 data is small and the errors are large by comparison making

an accurate determination impossible. We would have to rely entirely on a combination of neutron transport calculations and the Monte Carlo code to establish the baseline. This is the case with the smallest relative errors. Anything else we do to the data to split it into components would increase the relative errors.

For the $\times$ 10 case it is obvious from the raw data that there is a contribution from the Acrylic. Now, the number that we have to subtract to get the signal from the Sun is much larger. Thus we are much more sensitive to both statistical and systematic uncertainties. For $\times$ 1 the contribution is so small that even if we only know it to 50% it would not affect the final result by more than 5%. To get the same insensitivity for $\times$ 10 we would have to analyze at about 500 cm which wastes half the D_2O.

Figure 14 shows the theoretical limit which corresponds to the case where there is no uncertainty from the subtraction of the CC and the ES components. In the figure we have plotted just the NC component. Even here the statistical uncertainty limits us.

One of the best ways of splitting the data into components is to use the ratio R defined above. Figure 15 shows R as a function of radius for the no-oscillation case with a threshold of 50 hits. The dependence on the Monte Carlo is now much smaller since we are working with ratios of ratios. However, the errors are larger.

High energy background

It has been suggested that the high energy background can be determined from the light water in year 1. However this is difficult at best. Figure 16 shows the β-γ, the high energy and the elastic scattering components from year 1 with a radial cut of 650 cm to 850 cm and no cut on the angle. If we believe the Monte Carlo code, we have some sensitivity to the high energy background between 55 and 90 hits provided we can exclude the elastic scattering. Figure 17 (top) shows the total excluding the forward angle (channels 0 to 30 or $\cos\theta \leq 0.5$) scaled by $\frac{4}{3}$ to compensate for the different angular acceptance. This figure is essentially identical to figure

16b indicating that we indeed can fish out the high energy component. The bottom figure shows the high energy component alone inside the D_2O. The shapes (17a and 17) are not identical. This comes as no surprise since the response to *eg.* nonoenergetic electrons is quite different in the interior from that of the region where the reflectors are cutting off. We will therefore have great difficulty in determining the shape of the background in the D_2O from the H_2O data.

Conclusions

We have shown that provided both the 'internal' and the 'external' neutron backgrounds can be determined by independent means to 20% or better. a simple analysis which does not require fitting the shapes will tell us whether neutrino oscillations exists or not over a wide range of MSW parameters. We have also shown that the angular spectra alone will enable us to determine the relative amounts of Charged Current and Neutral Current even if the exact shape of the neutrino spectrum is not known.

Furthermore, it is clear that the Neutral Current data obtained in year 2 is not very useful to us and that perhaps one should think about adding Boron in some form (beads in suspension or on strings) to the D_2O in year 2. This would enable us to measure an unambiguous Charged Current spectrum.

References

[1] S.P. Rosen and J.M. Gelb, Private Comm.

[2] SNO-STR-88-126

[3] SNO-STR-89-01

[4] SNO-STR-89-43

[5] SNO-89-15

[6] SNO-STR-91-07

[7] W.F. Frati, Private Comm.

[8] S. Nozawa, Private Comm.

	Mass(tonnes)	Th(g/g)	U(g/g)
D_2O	1000	11×10^{-15}	11×10^{-15}
NaCl	2.5	1×10^{-12}	1×10^{-12}
Acrylic	30.0	1.9×10^{-12}	3.6×10^{-12}
H_2O	1667.7	22×10^{-15}	15×10^{-15}
PMT	7.5	0.1×10^{-6}	0.1×10^{-6}

Table 1: Masses and levels of ^{232}Th and ^{238}U in various detector components

Δm^2/ $\sin^2 2\theta$	Thres. N_{hit}	ES Fit	ES M.C.	Background Fit	Background M.C.	χ^2 (40 pts.)
	40	429 (29)	414	1621 (45)	1636	100.
vac.	50	279 (18)	297	144 (14)	125	58.6
	60	205 (15)	203	23 (6)	23	35.4
	70	122 (11)	123	5 (3)	4	27.8
	40	649 (33)	638	1625 (46)	1636	98.5
10^{-6}	50	444 (23)	454	135 (14)	125	60.1
0.01	60	311 (18)	309	21 (6)	23	44.1
	70	190 (14)	190	4 (3)	4	39.8
	40	78 (20)	67	1626 (44)	1636	93.7
10^{-5}	50	32 (8)	41	135 (13)	125	65.8
0.3	60	33 (6)	31	21 (5)	23	45.3
	70	22 (5)	21	3 (2)	4	32.8
	40	248 (25)	248	1636 (45)	1636	92.2
10^{-4}	50	114 (13)	128	139 (14)	125	57.6
0.01	60	59 (8)	64	28 (6)	23	38.6
	70	22 (5)	22	4 (3)	4	37.9

Table 2: Year 1 data for $0 \leq r \leq 600$ cm. Angular distribution fitted to $ES(\theta) \div$ constant.

Δm^2 / $\sin^2 2\theta$	Thres. N_{hit}	ES Fit	ES M.C.	CC Fit	CC M.C.	Background + NC Fit	Background + NC MC	χ^2 (40 pts.)
	40	465 (50)	410	3103 (536)	3256	2789 (566)	1657 + 103$\frac{1}{2}$	70.0
vac.	50	300 (36)	288	2432 (400)	2715	934 (419)	129 + 53$\frac{1}{2}$	63.6
	60	215 (29)	200	1926 (324)	2088	325 (338)	25 + 153	54.2
	70	139 (22)	134	1162 (229)	1467	332 (270)	8 + 24	43.5
	40	663 (57)	600	5011 (613)	4999	2615 (646)	1657 + 103$\frac{1}{2}$	61.1
10^{-6}	50	457 (44)	442	3955 (485)	4274	967 (507)	129 + 53$\frac{1}{2}$	53.6
0.01	60	307 (35)	306	2952 (405)	3372	596 (422)	25 + 153	52.4
	70	198 (28)	199	2142 (329)	2405	296 (342)	8 + 24	46.0
	40	97 (33)	73	709 (388)	580	2538 (411)	1657 + 103$\frac{1}{2}$	68.6
10^{-5}	50	40 (19)	49	355 (230)	506	823 (243)	129 + 53$\frac{1}{2}$	42.4
0.3	60	11 (12)	33	182 (161)	399	417 (169)	25 + 153	39.4
	70	7 (9)	19	115 (117)	283	213 (123)	8 + 24	34.5
	40	266 (42)	245	1907 (463)	1781	2543 (488)	1657 + 103$\frac{1}{2}$	72.1
10^{-4}	50	105 (24)	121	846 (271)	907	741 (285)	129 + 53$\frac{1}{2}$	57.5
0.01	60	34 (13)	52	300 (158)	360	256 (166)	25 + 153	59.6
	70	11 (8)	22	93 (92)	153	103 (96)	8 + 24	27.1

Table 3: Year 2 data for 0≤r≤600 cm. Angular distribution fitted to ES(θ) ÷ [1 + $\frac{1}{3}$ cos θ] + constant.

Δm^2/ $\sin^2 2\theta$	Thres. N_{hit}	ES Fit	ES M.C.	CC Fit	CC M.C.	Background + NC Fit	Background + NC MC	χ^2 (40 pts.)
	40	440 (60)	427	2971 (673)	3282	6636 (713)	1677 + 4661	48.2
vac.	50	311 (47)	297	2863 (550)	2788	3766 (579)	139 + 3715	31.4
	60	229 (38)	191	2191 (453)	2203	2410 (475)	30 + 2406	27.2
	70	129 (27)	118	1576 (345)	1573	1188 (360)	10 + 1192	32.2
	40	669 (66)	633	4851 (734)	4940	6391 (775)	1677 + 4661	26.5
10^{-6}	50	494 (53)	440	4368 (609)	4205	3637 (640)	139 + 3715	20.9
0.01	60	359 (43)	307	3356 (507)	3308	2336 (531)	30 + 2406	21.4
	70	232 (32)	203	2395 (396)	2401	1179 (413)	10 + 1192	24.2
	40	108 (47)	69	1089 (561)	582	5792 (595)	1677 + 4661	57.8
10^{-5}	50	64 (35)	48	960 (437)	496	3374 (461)	139 + 3715	30.4
0.3	60	78 (28)	36	719 (347)	375	2050 (366)	30 + 2406	25.7
	70	39 (19)	19	536 (247)	263	909 (258)	10 + 1192	39.7
	40	180 (52)	205	1222 (614)	1842	6983 (652)	1677 + 4661	46.2
10^{-4}	50	116 (38)	114	1188 (463)	978	3642 (489)	139 + 3715	23.2
0.01	60	107 (29)	66	864 (352)	422	1953 (370)	30 + 2406	20.3
	70	35 (18)	26	412 (238)	150	932 (249)	10 + 1192	42.7

Table 4: Year 3 data for $0 \leq r \leq 600$ cm. Angular distribution fitted to ES(θ) + [$1 + \frac{1}{3} \cos\theta$] + constant.

Δm^2/ $\sin^2 2\theta$	Thres. N_{hit}	Year 1 ES	Year 2 ES	Year 2 CC	Year 2 NC	Year 3 ES	Year 3 CC	Year 3 NC
	40	1.04 (.07)	1.13 (.12)	.95 (.16)	1.0 (.2)	1.03 (.14)	.91 (.21)	1.05 (.11)
vac.	50	0.94 (.06)	1.04 (.13)	.90 (.15)	1.4 (.6)	1.05 (.16)	1.03 (.20)	0.98 (.15)
	60	1.01 (.07)	1.08 (.15)	.92 (.16)	1.8 (1.9)	1.20 (.20)	0.99 (.21)	0.99 (.12)
	70	0.99 (.09)	1.04 (.16)	.79 (.16)	10. (8.)	1.09 (.23)	1.00 (.22)	0.99 (.30)
	40	1.02 (.05)	1.11 (.10)	1.00 (.12)	1.0 (.2)	1.06 (.10)	0.98 (.15)	1.01 (.12)
10^{-6}	50	0.98 (.05)	1.03 (.10)	0.93 (.11)	1.5 (.8)	1.12 (.12)	1.04 (.14)	0.94 (.17)
.01	60	1.01 (.06)	1.00 (.11)	0.88 (.12)	3.3 (2.4)	1.17 (.14)	1.01 (.15)	0.96 (.22)
	70	1.00 (.07)	0.99 (.14)	0.89 (.14)	9. (11.)	1.14 (.16)	1.00 (.16)	0.98 (.34)
	40	1.16 (.30)	1.33 (.45)	1.22 (.67)	0.94 (.15)	1.6 (.7)	1.9 (1.0)	0.91 (.09)
10^{-5}	50	0.78 (.20)	0.82 (.48)	1.2 (.4)	2.1 (0.6)	1.3 (.7)	2.0 (.9)	0.88 (.12)
0.3	60	1.06 (.19)	0.33 (.36)	0.46 (.40)	2.3 (1.9)	2.2 (.8)	1.9 (.9)	.84 (.15)
	70	1.05 (.24)	0.37 (.47)	0.41 (.41)	6.7 (3.8)	2.1 (1.)	2.0 (.9)	.76 (.21)
10^{-4}	40	1.00 (.10)	1.09 (.17)	1.07 (.26)	.95 (.18)	0.88 (.25)	.98 (.33)	1.10 (.10)
.01	50	0.89 (.10)	0.86 (.19)	0.93 (.30)	1.1 (.4)	1.02 (.33)	1.21 (.47)	0.94 (.13)
	60	0.92 (.13)	0.65 (.25)	0.83 (.44)	1.4 (.9)	1.62 (.44)	2.0 (.8)	0.80 (.15)
	70	1.00 (.23)	0.50 (.36)	0.61 (.60)	3. (3.)	1.4 (.7)	2.7 (1.6)	0.78 (.21)

Table 5: Ratios of fitted numbers to Monte Carlo input numbers for r $\leq$ 600 cm

Threshold		ES	CC	NC	
N_{hit}	E(MeV)			D_2O	NaCl
40	4.2	1254	9903	769	3225
50	5.3	909	8310	395	2543
60	6.3	640	6474	109	1662
70	7.3	425	4634	14	869

Table 6: Expected rates based on multiyear distributions inside r = 600 cm for Standard Solar Model with 5.8×10^6 ν_e per cm^2 per sec.

Δm^2/ $\sin^2 2\theta$	Thres. N_{hit}	Year 1 ES	Year 2 ES	Year 2 CC	Year 2 NC	Year 3 ES	Year 3 CC	Year 3 NC
vac.	40	.34 (.02)	.37 (.04)	.31 (.05)	3.6 (0.7)	.35 (.05)	.30 (.07)	2.1 (0.2)
	50	.31 (.02)	.33 (.04)	.29 (.05)	2.4 (1.1)	.34 (.05)	.34 (.07)	1.5 (0.2)
	60	.32 (.02)	.34 (.05)	.30 (.05)	3.0 (3.1)	.36 (.06)	.34 (.07)	1.5 (0.3)
	70	.29 (.03)	.33 (.05)	.25 (.06)	24. (19.)	.30 (.06)	.34 (.07)	1.4 (0.4)
10^{-6} .01	40	.52 (.03)	.53 (.05)	.51 (.06)	3.4 (0.8)	.53 (.05)	.49 (.07)	2.0 (0.2)
	50	.49 (.03)	.50 (.05)	.48 (.06)	2.5 (1.3)	.54 (.06)	.53 (.07)	1.4 (0.3)
	60	.49 (.03)	.48 (.05)	.46 (.06)	5.5 (3.9)	.56 (.07)	.52 (.08)	1.4 (0.3)
	70	.45 (.03)	.47 (.07)	.46 (.07)	21. (24.)	.55 (.08)	.52 (.09)	1.4 (0.5)
10^{-5} 0.3	40	.06 (.02)	.06 (.02)	.07 (.04)	3.3 (0.5)	.09 (.04)	.11 (.06)	1.8 (0.2)
	50	.04 (.01)	.05 (.02)	.04 (.03)	2.1 (0.6)	.07 (.04)	.12 (.05)	1.3 (0.2)
	60	.05 (.01)	.02 (.02)	.03 (.03)	3.8 (1.6)	.12 (.04)	.11 (.05)	1.2 (0.2)
	70	.05 (.01)	.01 (.01)	.02 (.02)	15. (9.)	.09 (.04)	.12 (.06)	1.1 (0.3)
10^{-4} .01	40	.20 (.02)	.21 (.03)	.19 (.05)	3.3 (0.6)	.14 (.04)	.12 (.06)	2.2 (0.2)
	50	.13 (.01)	.12 (.03)	.10 (.03)	1.9 (0.7)	.13 (.04)	.14 (.05)	1.4 (0.2)
	60	.09 (.01)	.05 (.02)	.05 (.03)	2.4 (1.5)	.17 (.05)	.13 (.05)	1.2 (0.2)
	70	.05 (.01)	.03 (.02)	.02 (.02)	7.4 (6.9)	.08 (.04)	.09 (.05)	0.9 (0.3)

Table 7: Ratios of fitted numbers to numbers expected from the Standard Solar Model with a ν_e flux of 5.8×10^6 cm^{-2} s^{-1} for r $\leq$ 600 cm

Δm^2/ $\sin^2 2\theta$	Thres. N_{hit}	ES Fit	ES M.C.	Background Fit	Background M.C.	χ^2 (40 pts.)
	40	382 (23)	391	395 (423)	385	139.4
10^{-6}	50	275 (17)	281	17 (6)	11	46.2
0.01	60	191 (14)	190	1 (2)	1	36.1
	70	123 (11)	123	1 (1)	1	37.0

Table 8: Year 1 data for 0≤r≤500 cm. Angular distribution fitted to ES(θ) + constant.

Δm^2/ $\sin^2 2\theta$	Thres. N_{hit}	ES Fit	ES M.C.	CC Fit	CC M.C.	Background + NC Fit	Background + NC MC	χ^2 (40 pts.)
	40	346 (42)	375	2635 (460)	3126	1686 (485)	392 + 773	43.3
10^{-6}	50	254 (34)	275	2257 (384)	2680	870 (402)	10 + 416	40.4
0.01	60	149 (27)	190	1554 (322)	2118	727 (336)	1 + 121	43.1
	70	103 (22)	127	1173 (264)	1542	415 (275)	0 + 22	37.7

Table 9: Year 2 data for 0≤r≤500 cm. Angular distribution fitted to ES(θ) + [$1 + \frac{1}{3}\cos\theta$] + constant.

Δm^2/ $\sin^2 2\theta$	Thres. N_{hit}	ES Fit	ES M.C.	CC Fit	CC M.C.	Background + NC Fit	Background + NC MC	χ^2 (40 pts.)
	40	394 (50)	380	3416 (559)	3096	3081 (590)	401 + 3013	23.0
10^{-6}	50	307 (41)	268	3196 (484)	2646	1860 (507)	12 + 2437	24.1
0.01	60	243 (35)	189	2555 (410)	2137	1158 (429)	3 + 1627	26.9
	70	164 (27)	131	1650 (325)	1591	747 (339)	1 + 838	25.1

Table 10: Year 3 data for 0≤r≤500 cm. Angular distribution fitted to ES(θ) + [$1 + \frac{1}{3}\cos\theta$] + constant.

Threshold		ES	CC	NC	
N_{hit}	E(MeV)			D_2O	NaCl
40	4.2	768	6211	597	2233
50	5.3	566	5260	314	1790
60	6.3	407	4162	90	1191
70	7.3	275	3052	12	642

Table 11: Expected rates based on multiyear distributions inside r = 500 cm for Standard Solar Model with 5.8×10^6 ν_e per cm^2 per sec.

Δm^2 / $\sin^2 2\theta$	Thres. N_{hit}	Year 1 ES	Year 2 ES	Year 2 CC	Year 2 NC	Year 3 ES	Year 3 CC	Year 3 NC
	40	.50 (.03)	.45 (.05)	.42 (.07)	2.8 (0.8)	.51 (.07)	.55 (.09)	1.4 (0.3)
10^{-6}	50	.49 (.03)	.49 (.06)	.43 (.07)	2.8 (1.3)	.54 (.07)	.61 (.09)	1.0 (0.3)
.01	60	.47 (.03)	.37 (.07)	.37 (.08)	8.1 (3.7)	.60 (.09)	.61 (.10)	1.0 (0.4)
	70	.45 (.04)	.37 (.08)	.38 (.09)	35. (23.)	.60 (.10)	.54 (.11)	1.2 (0.5)

Table 12: Ratios of fitted numbers to numbers expected from the Standard Solar Model with a ν_e flux of 5.8×10^6 cm^{-2} s^{-1} for r $\leq$ 500 cm.

Hamamatsu 8" , 3.8 ns

Fig. 1

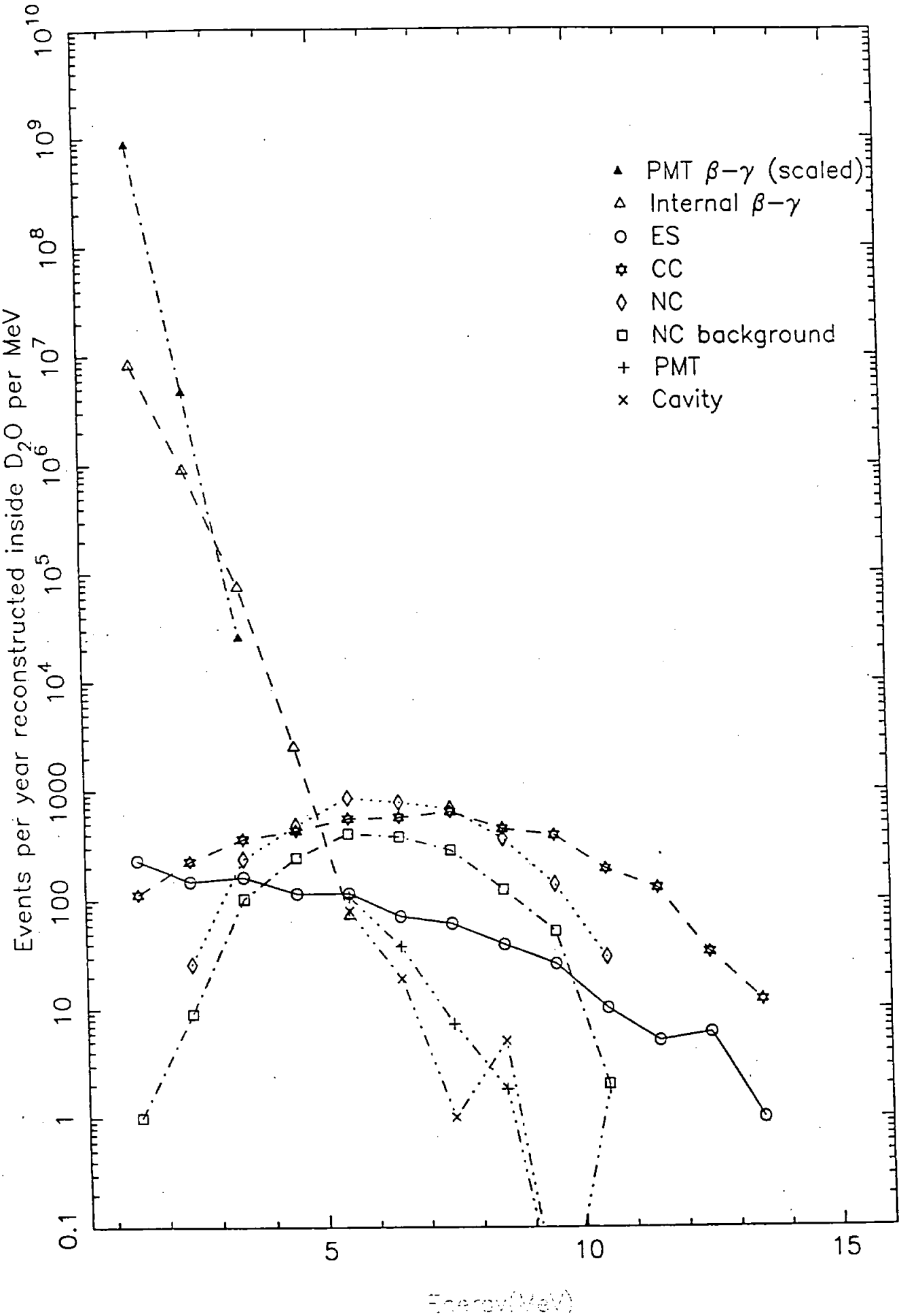

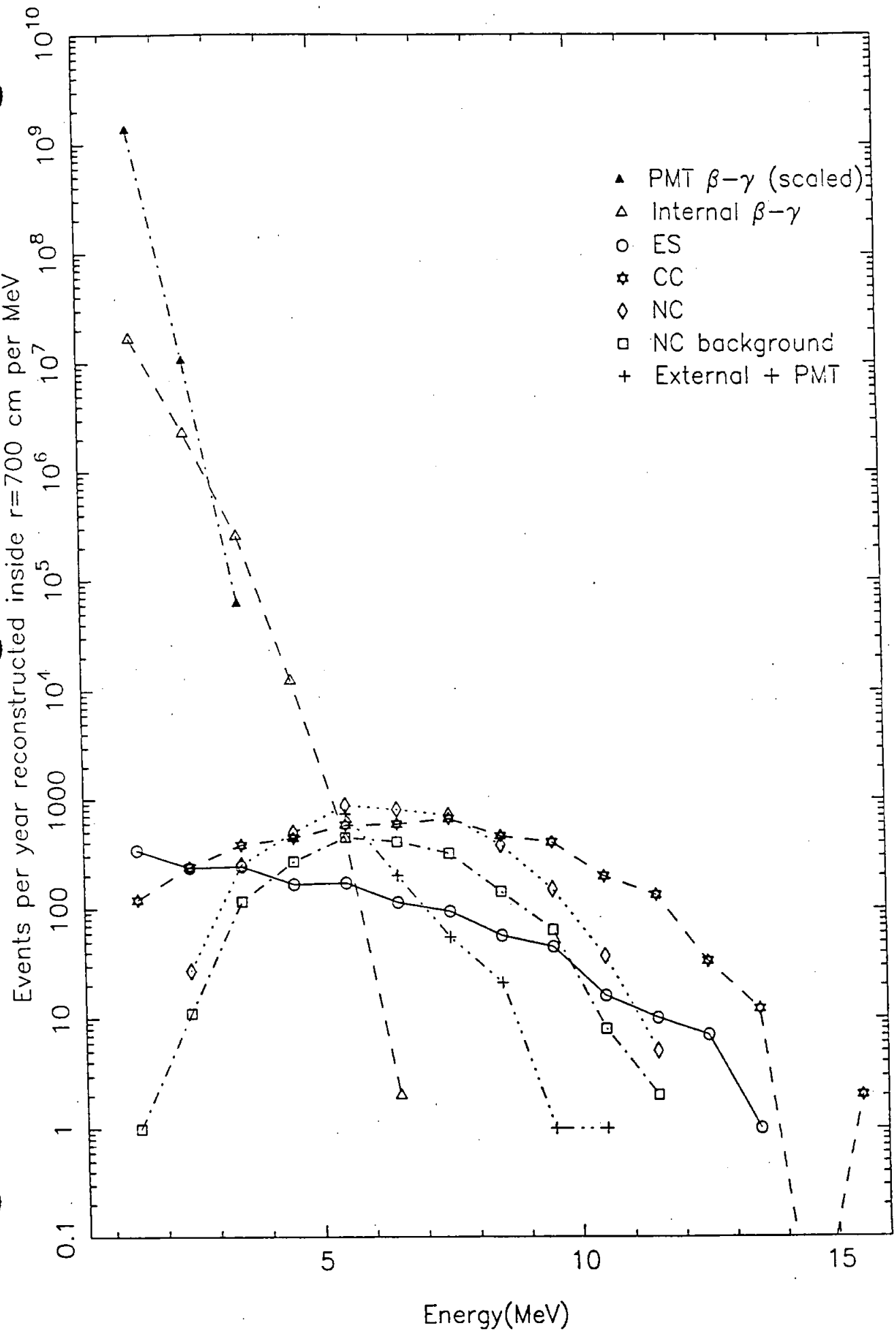
Hamamatsu 8" , 3.8 ns
PMT β−γ (scaled)
Internal β−γ
ES
CC
NC
NC background
External + PMT
Events per year reconstructed inside r=700 cm per MeV
Energy(MeV)
0.1
1
10
100
1000
10^4
10^5
10^6
10^7
10^8
10^9
10^10
5
10
15

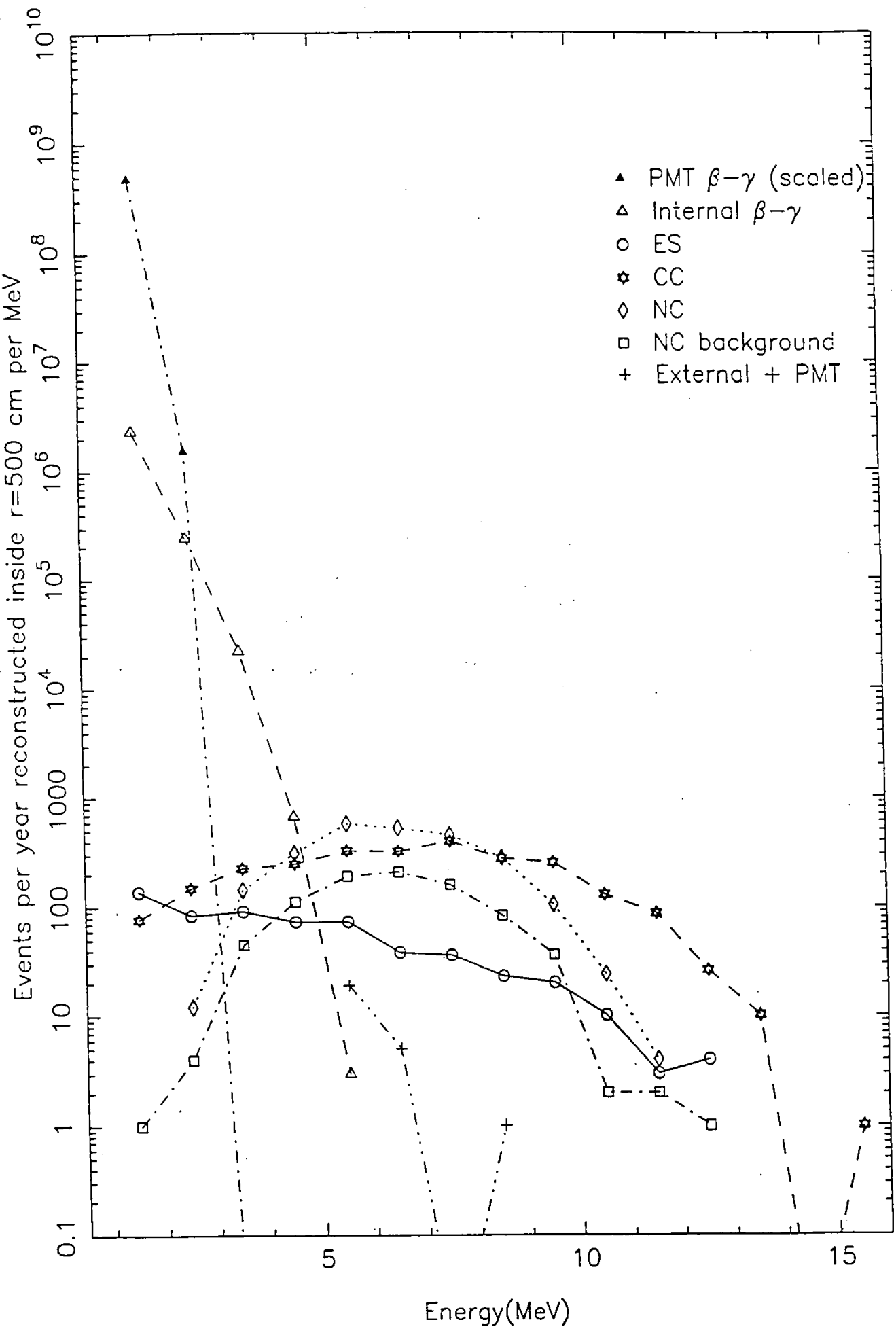
Hamamatsu 8" , 3.8 ns
PMT β−γ (scaled)
Internal β−γ
ES
CC
NC
NC background
External + PMT
Events per year reconstructed inside r=500 cm per MeV
Energy(MeV)
0.1
1
10
100
1000
10^4
10^5
10^6
10^7
10^8
10^9
10^10
5
10
15

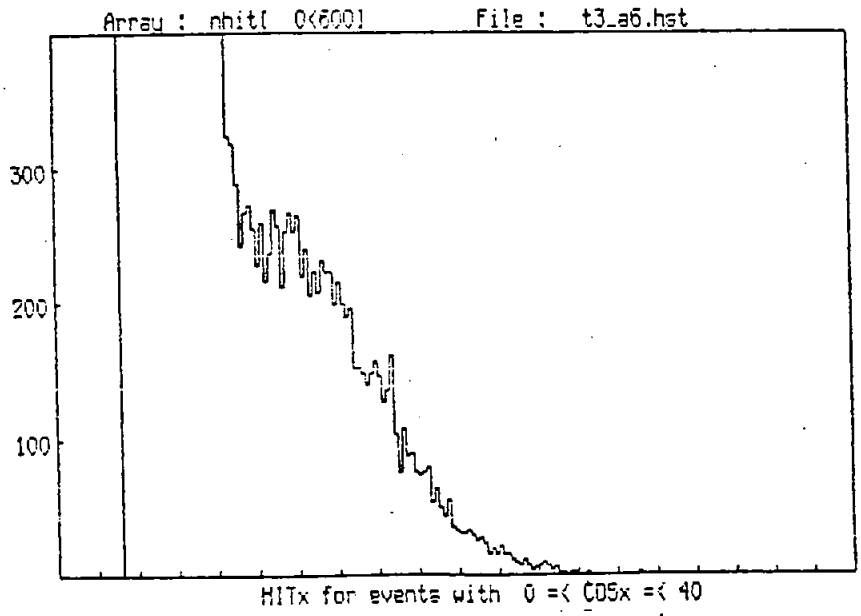
Array : nhit[0<600]
File : t3_a6.hst
300
200
100
HITx for events with 0 =< COSx =< 40

Fig 4a

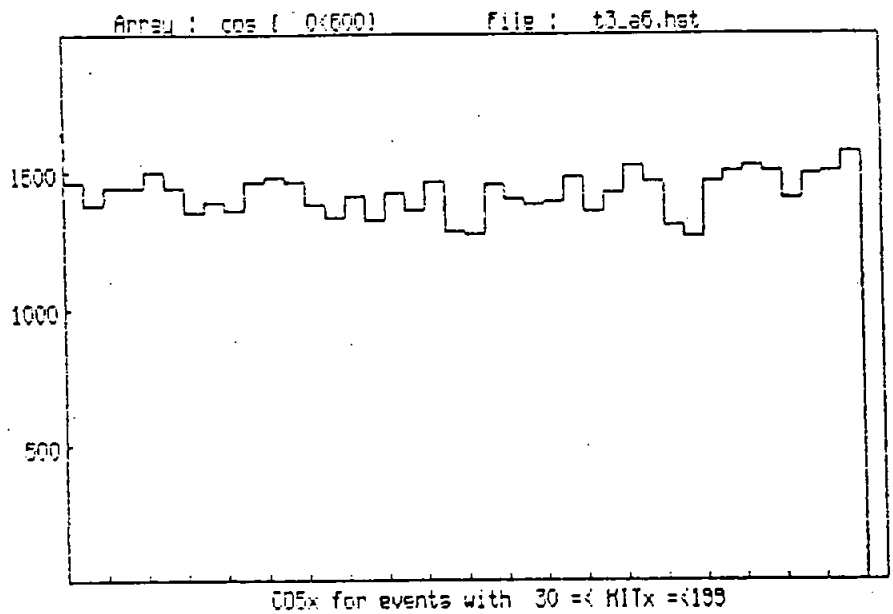
Array : cos [0<600]
File : t3_a6.hst
1500
1000
500
COSx for events with 30 =< HITx =<199

4b

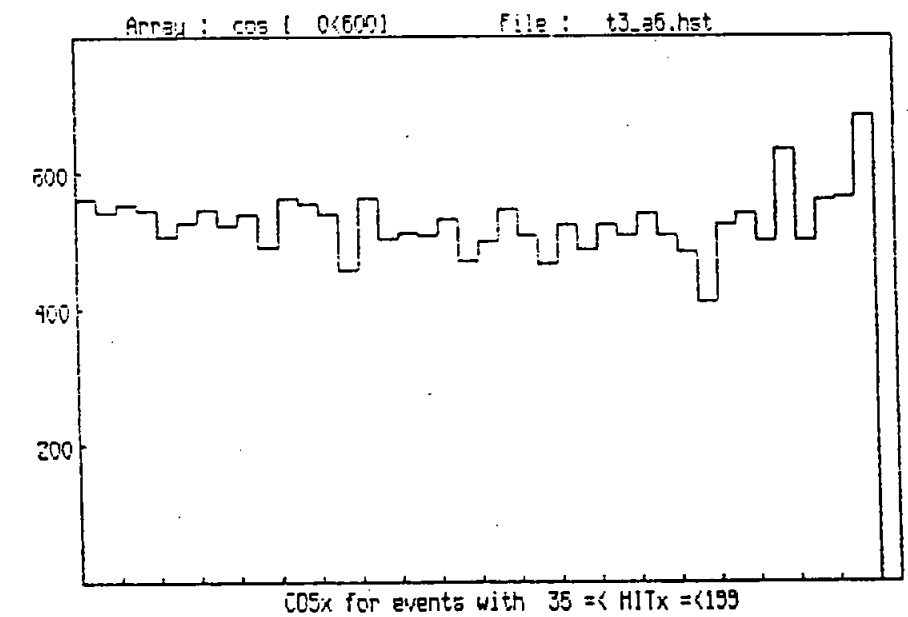
Array : cos [0<600]
File : t3_a6.hst
600
400
200
COSx for events with 35 =< HITx =<199

4c

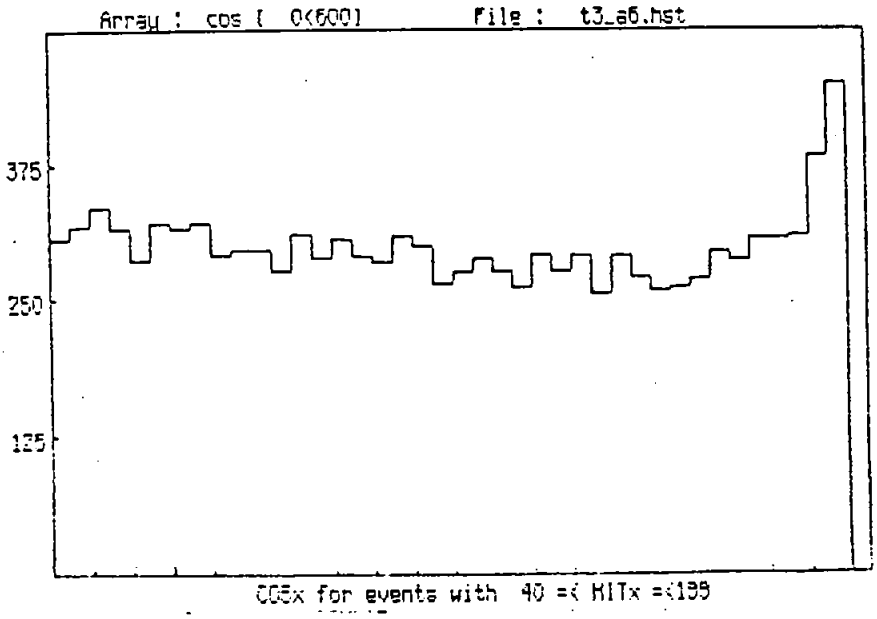
Array : cos [0(600]
File : t3_a6.hst
375
250
125
COSx for events with 40 =< HITx =<199

4d

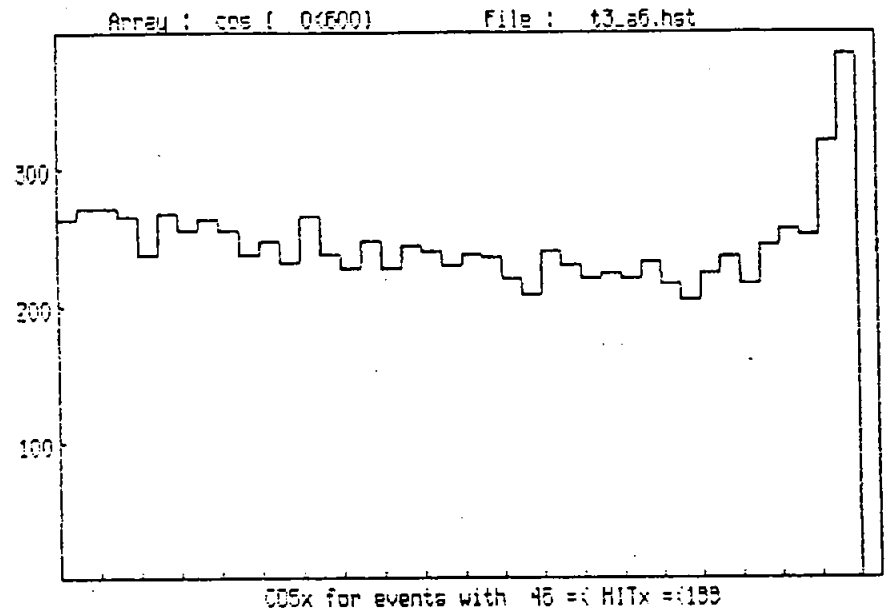
Array : cos [0(600]
File : t3_a6.hst
300
200
100
COSx for events with 45 =< HITx =<199

4e

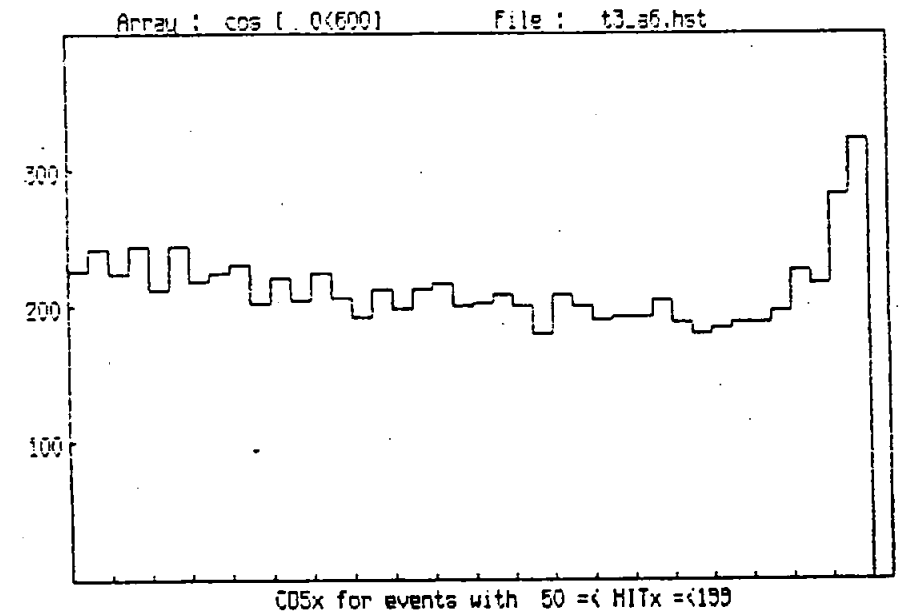
Array : cos [0(600]
File : t3_a6.hst
300
200
100
COSx for events with 50 =< HITx =<199

4f

4g

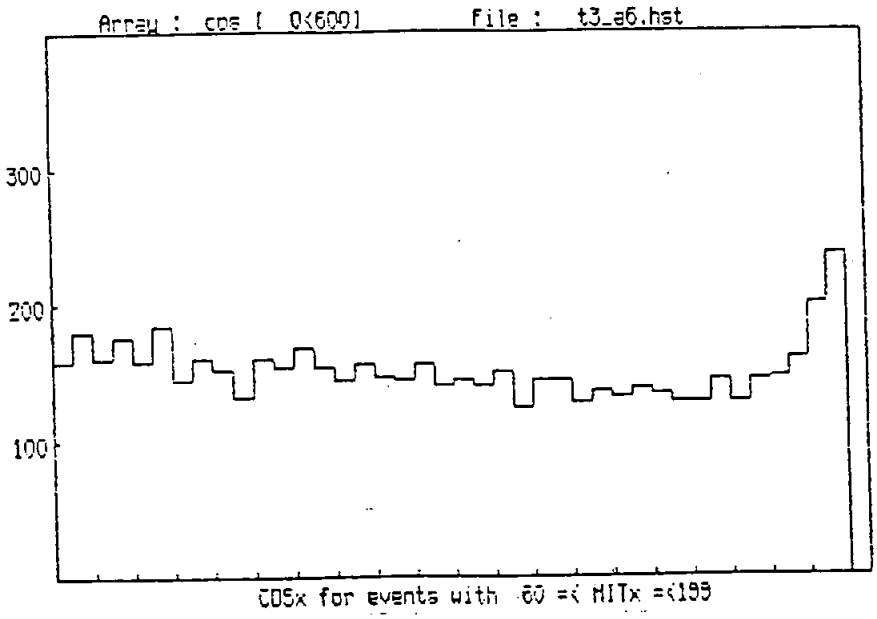
Array : cos [0<600]
File : t3_a6.hst
300
200
100
COSx for events with 60 =< HITx =<199

4h

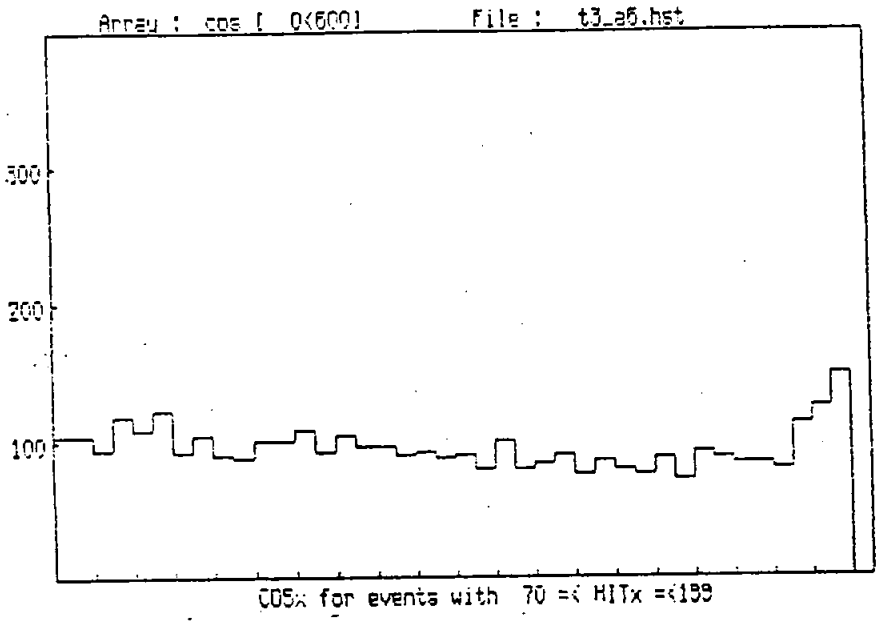
Array : cos [0<600]
File : t3_a6.hst
300
200
100
COSx for events with 70 =< HITx =<199

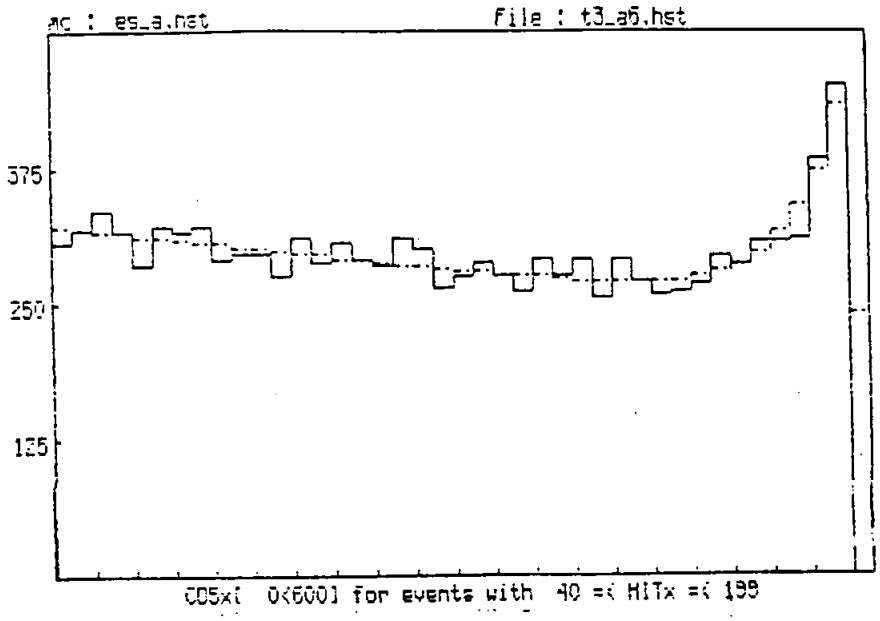
ac : es_a.hst
File : t3_a6.hst
375
250
125
C05x[0<600] for events with 40 =< HITx =< 199

Fig 5a

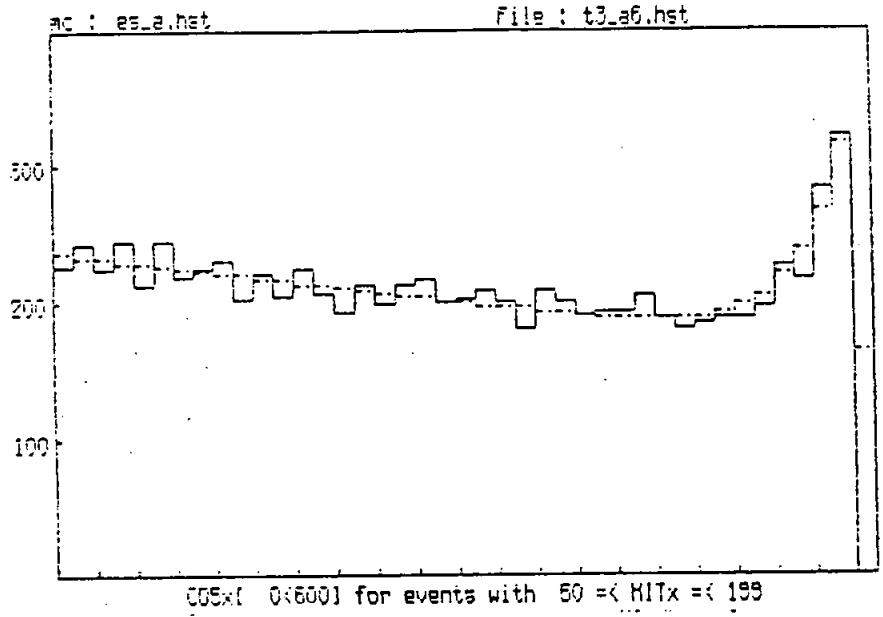
ac : es_a.hst
File : t3_a6.hst
300
200
100
C05x[0<600] for events with 50 =< HITx =< 199

5b

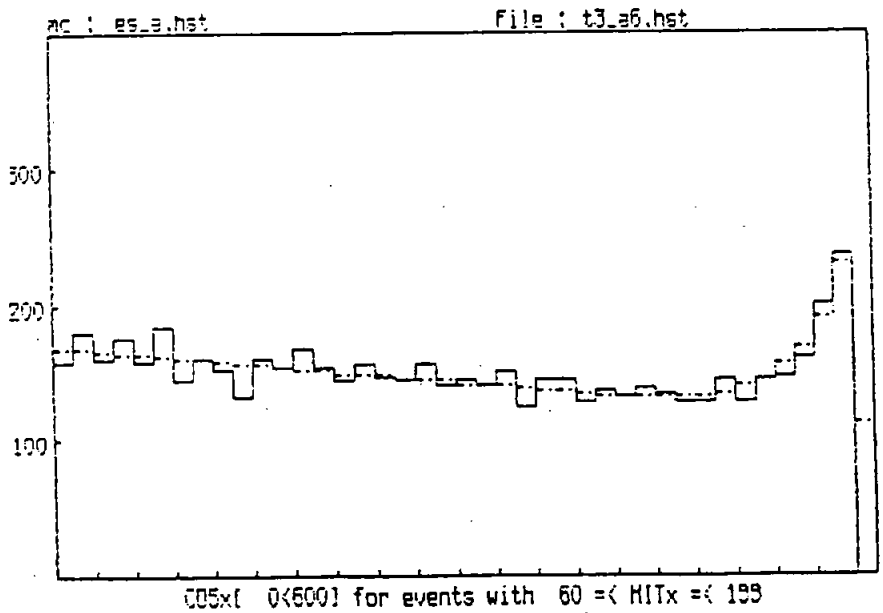
ac : es_a.hst
File : t3_a6.hst
300
200
100
C05x[0<600] for events with 60 =< HITx =< 199

5c

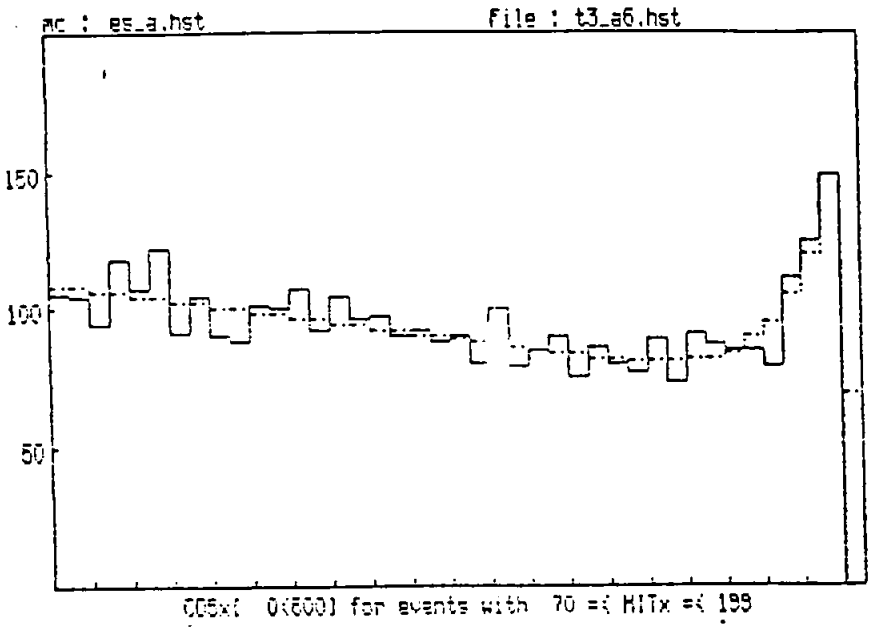
mc : es_a.hst
File : t3_a6.hst
150
100
50
CDSx[0:600] for events with 70 =< HITx =< 198

Fig 6

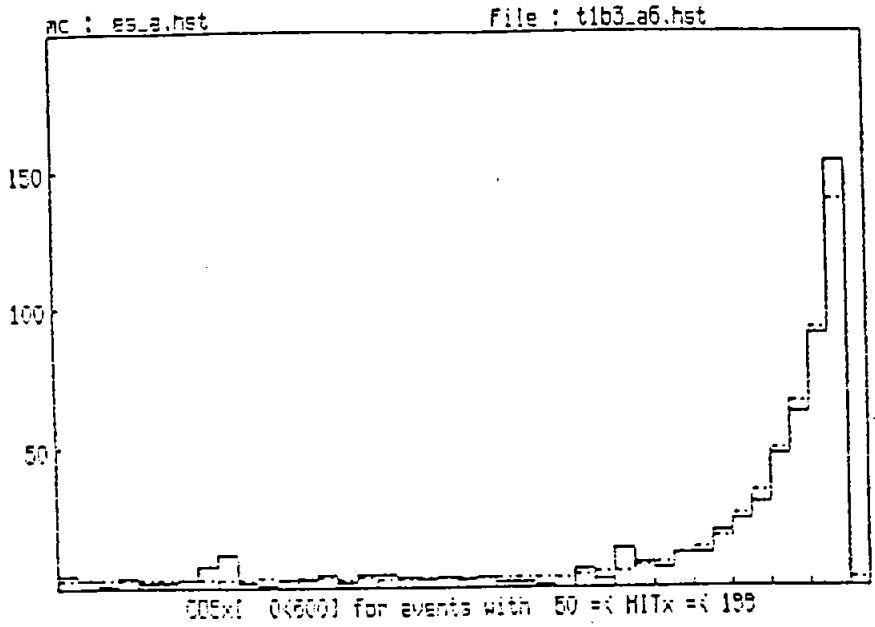

year 1

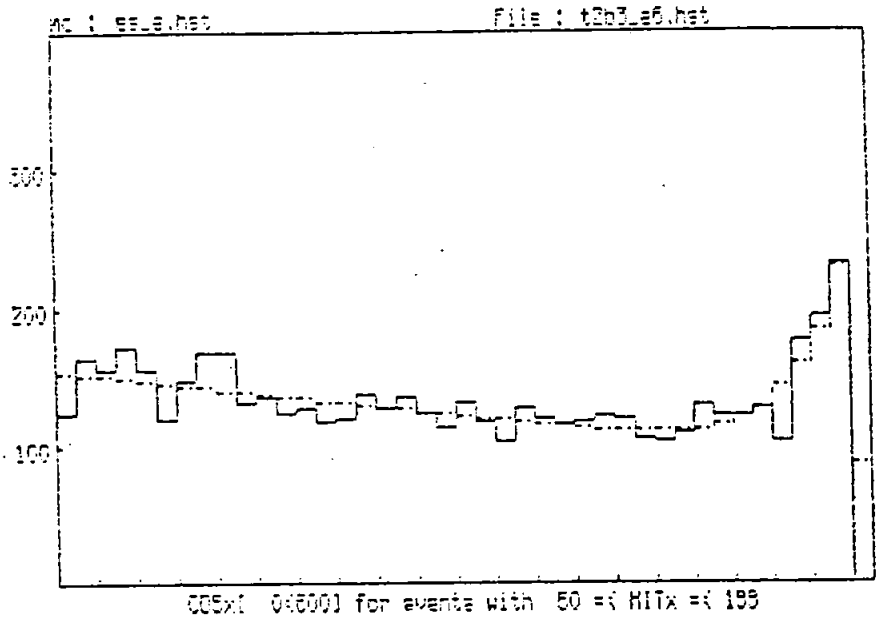

year 2

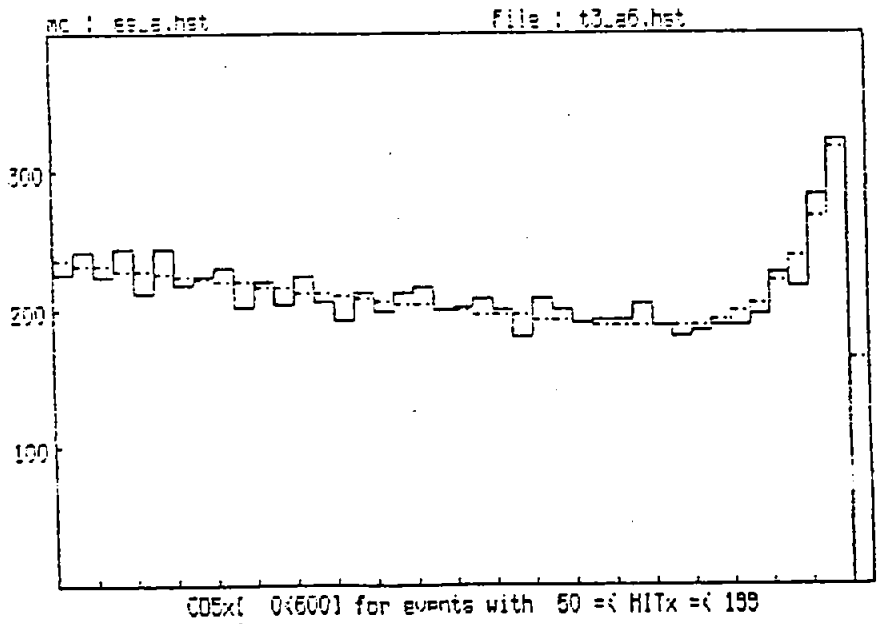

year 3

Fig 7

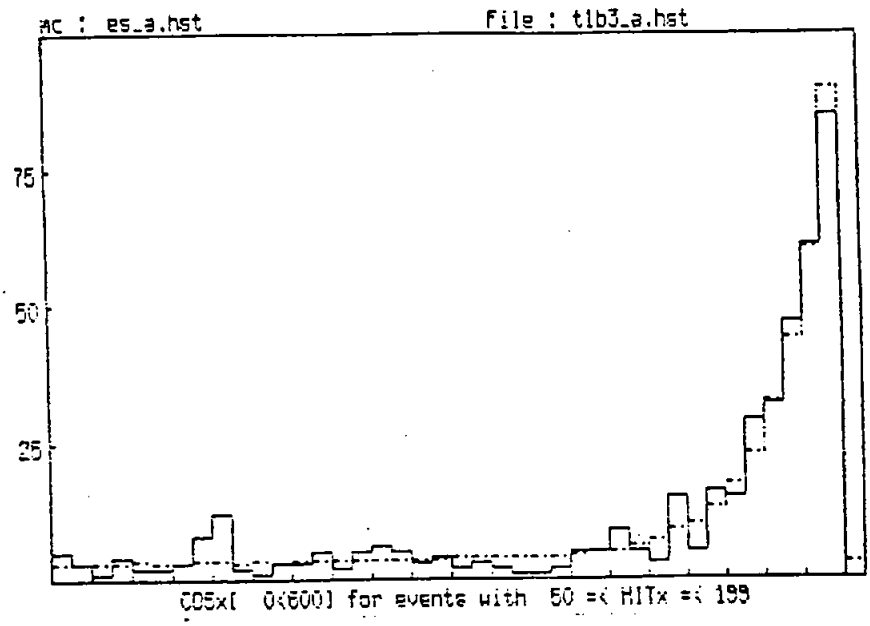

yew 1

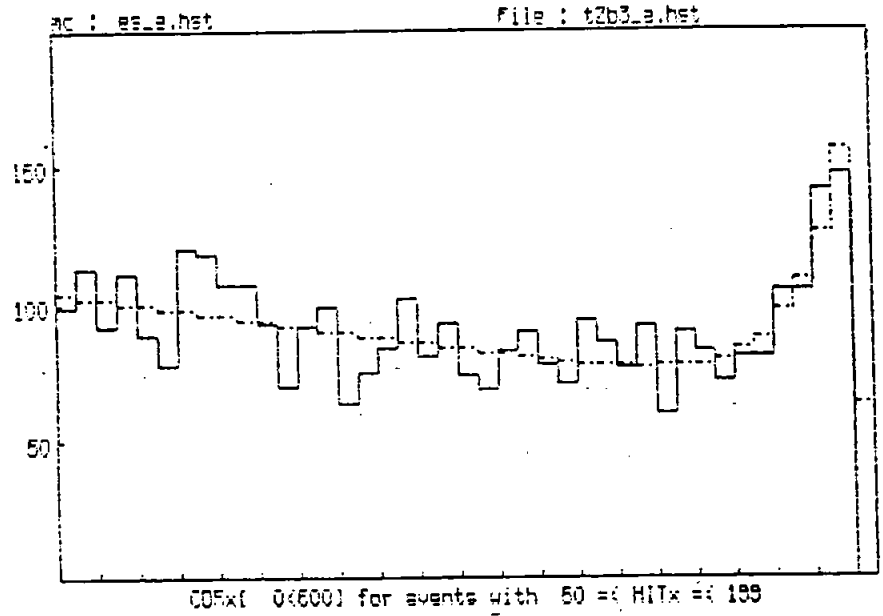

yew 2

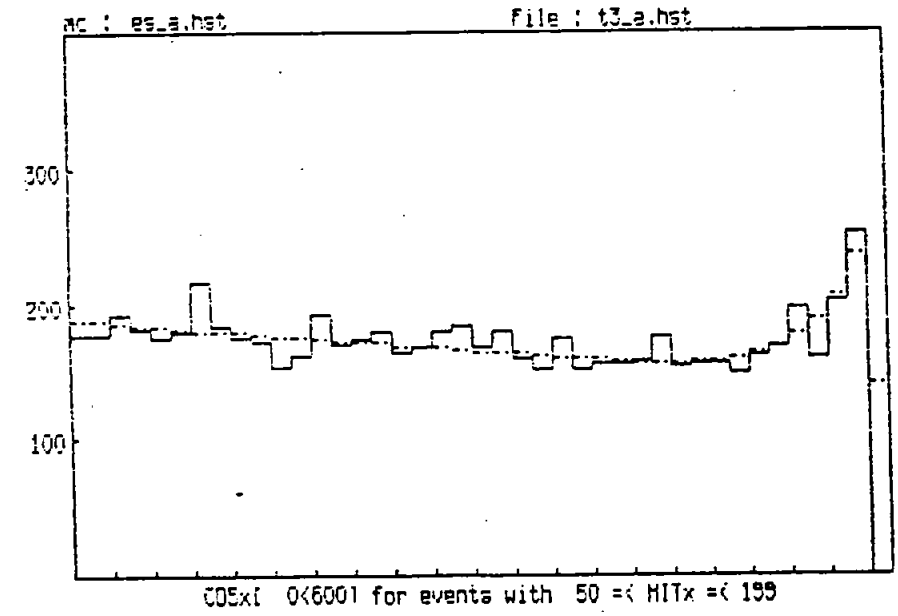

yew 3

Fig. 8

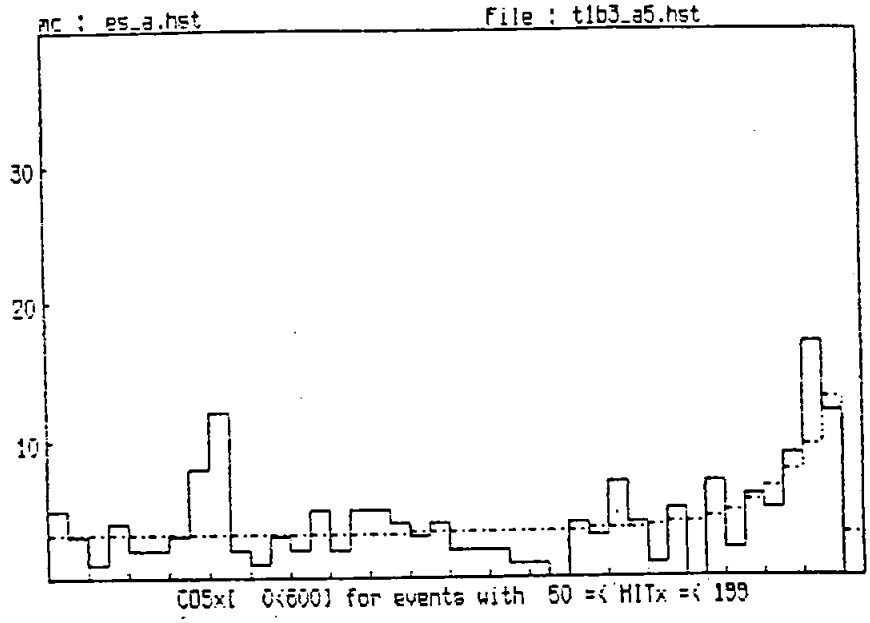

yew 1

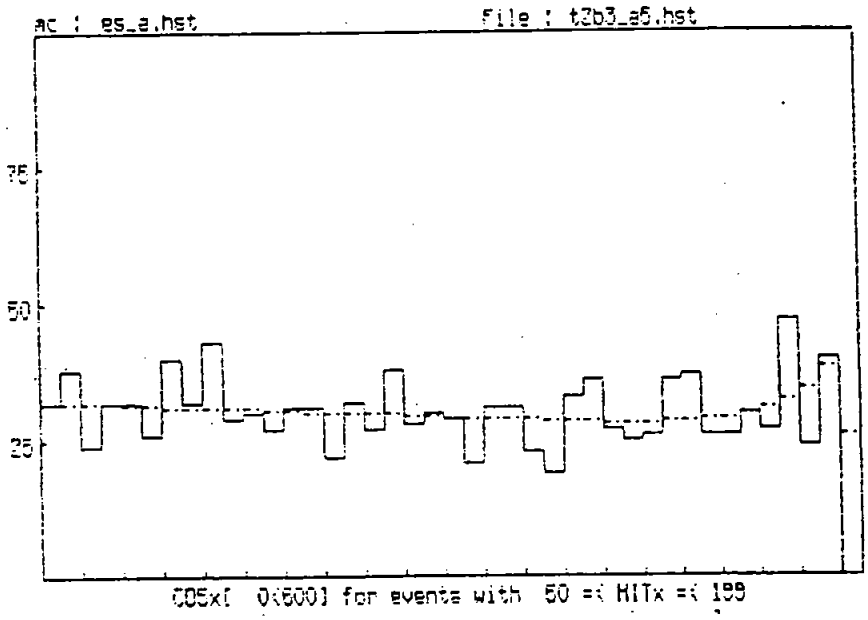

yew 2

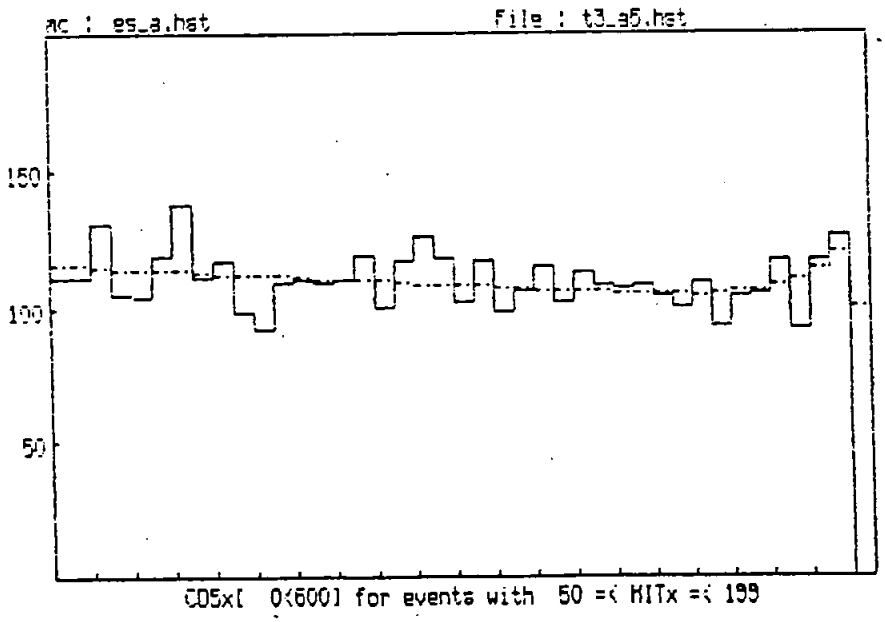

yew 3

Fig. 9

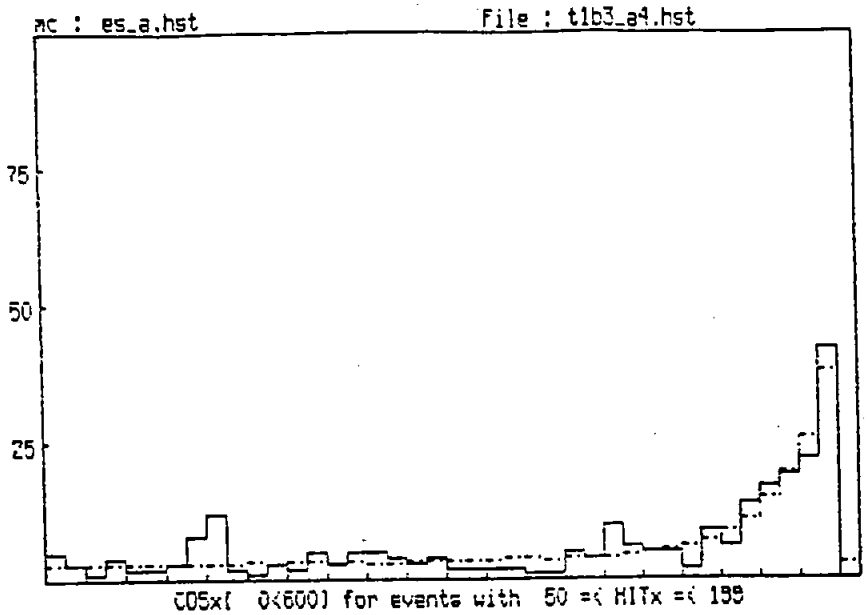

year 1

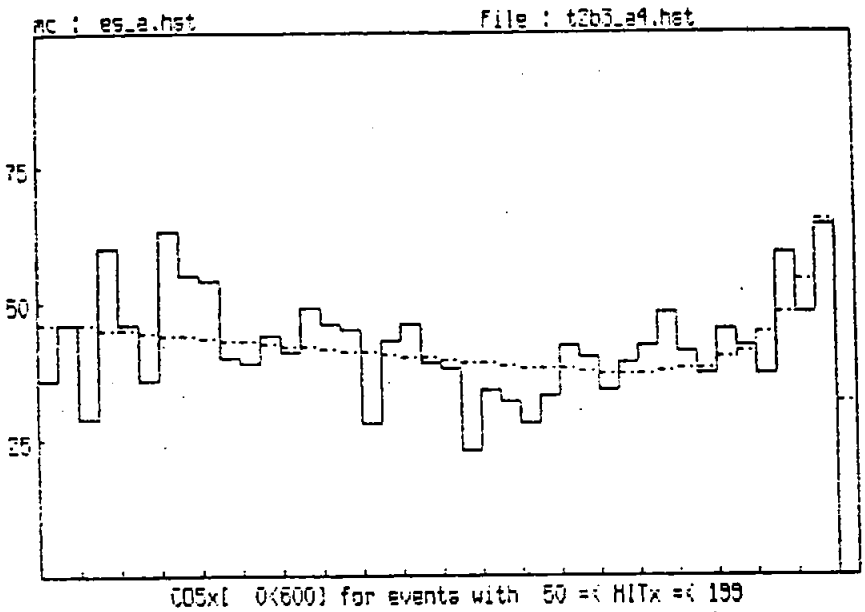

year 2

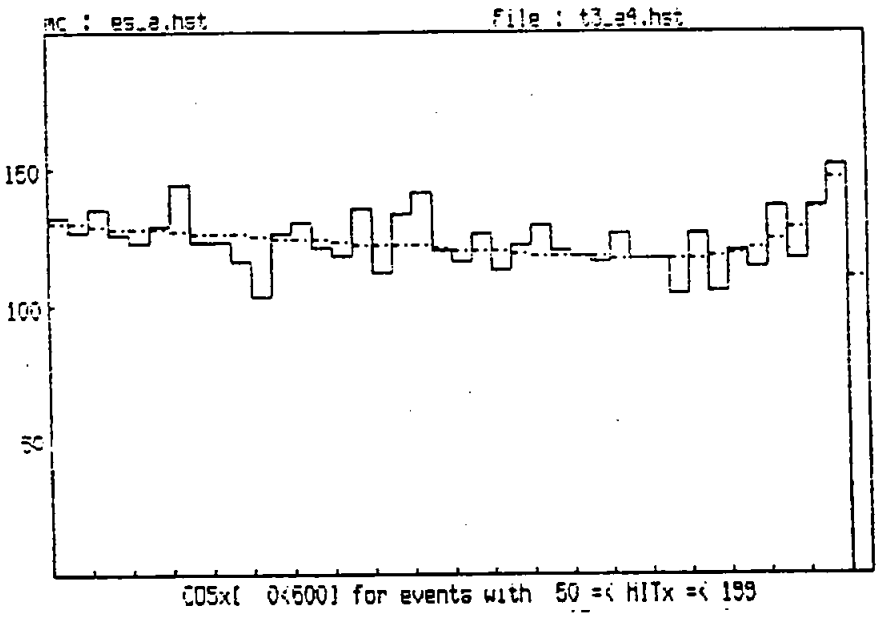

year 3

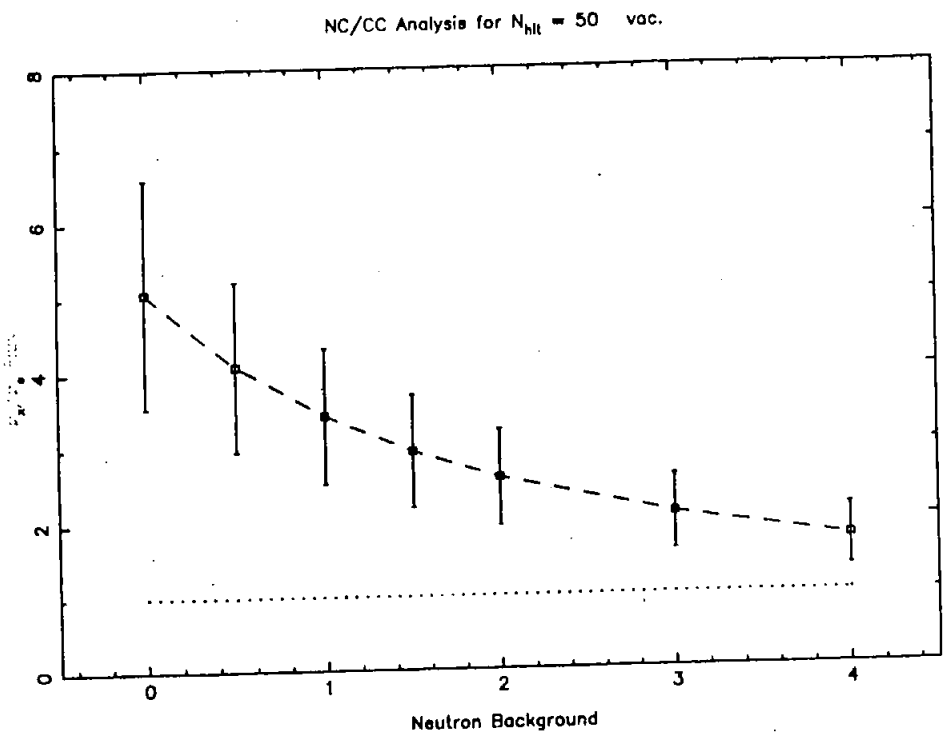
NC/CC Analysis for N_{hlt} = 50 vac.
ν_x/ν_e Flux
Neutron Background

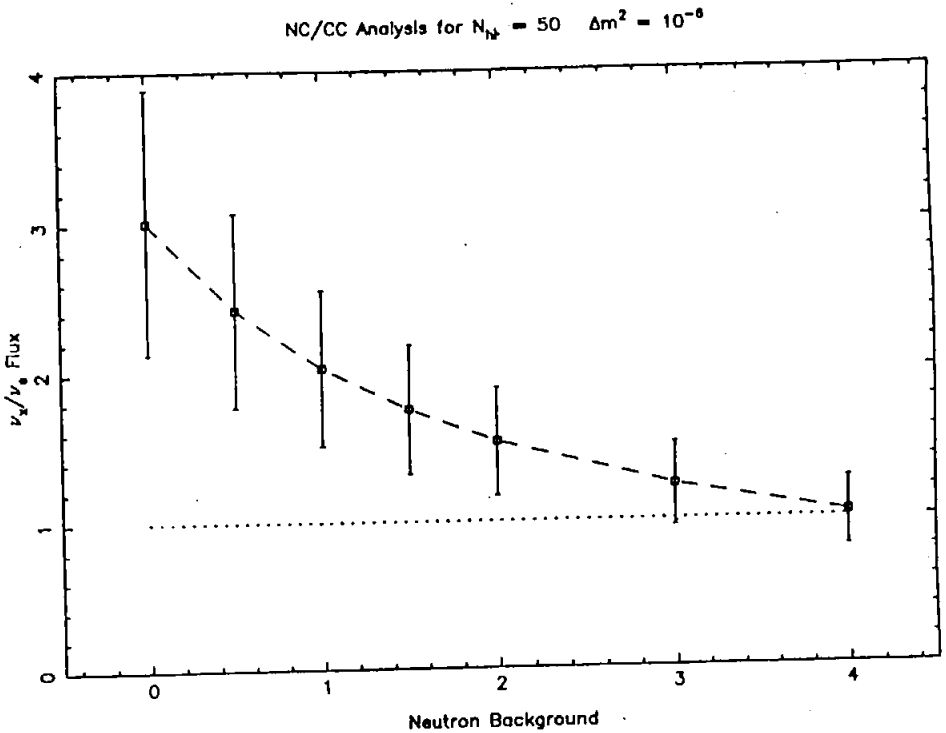
NC/CC Analysis for N_{hl} = 50 $\Delta m^2 = 10^{-6}$
ν_x/ν_e Flux
Neutron Background

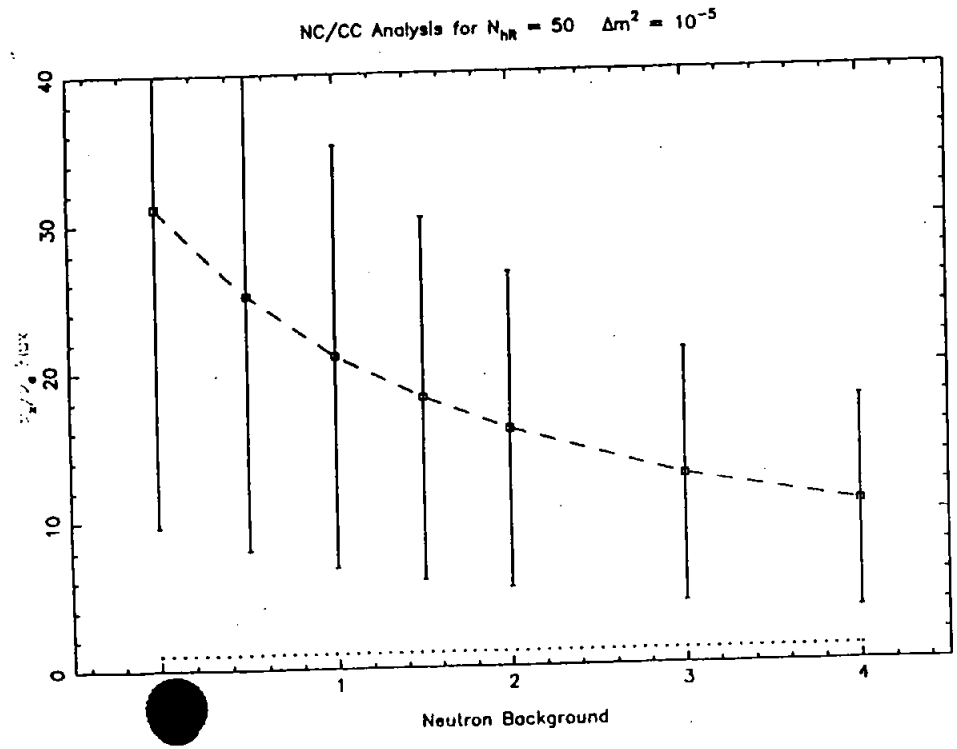
NC/CC Analysis for N_{hR} = 50 $\Delta m^2 = 10^{-5}$
Neutron Background

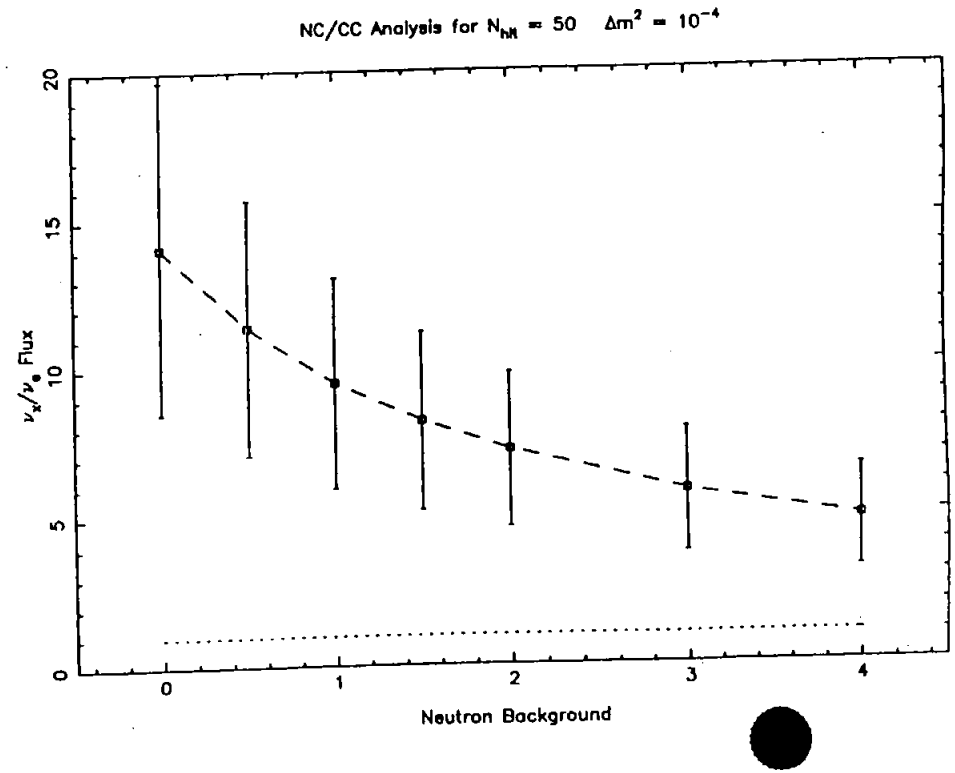
NC/CC Analysis for N_{hR} = 50 $\Delta m^2 = 10^{-4}$
ν_x/ν_e Flux
Neutron Background

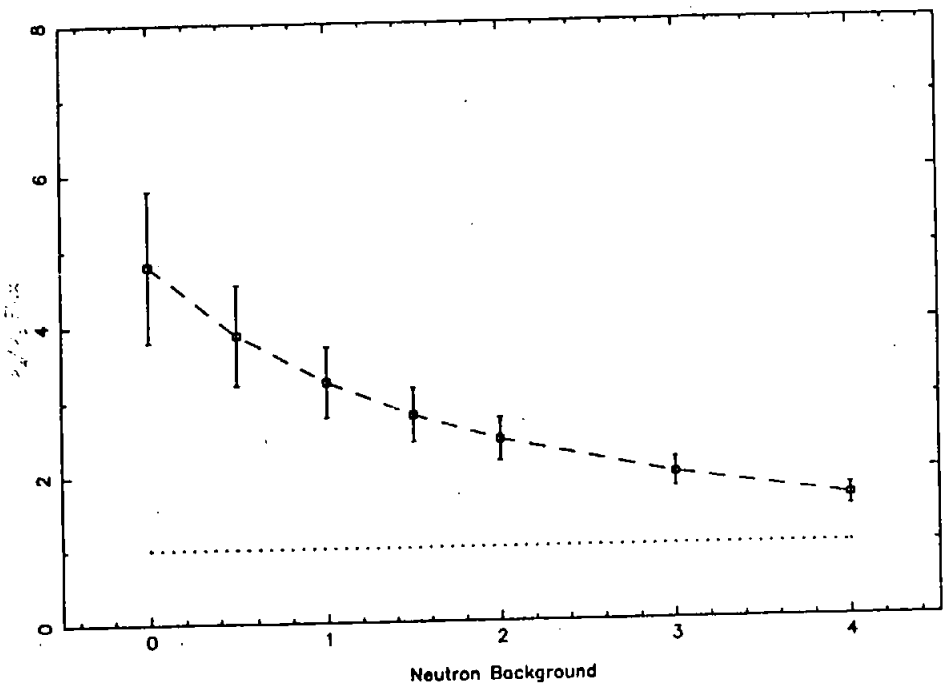
NC/CC Analysis for N_{hlt} = 50 vac.
Neutron Background

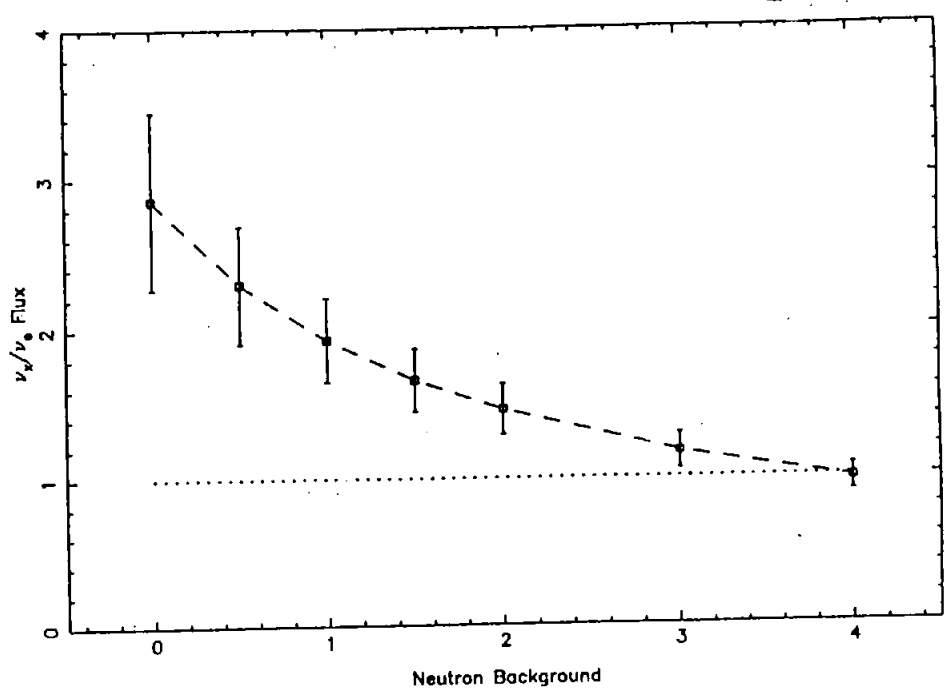
NC/CC Analysis for N_{hlt} = 50 $\Delta m^2 = 10^{-6}$
ν_x/ν_e Flux
Neutron Background

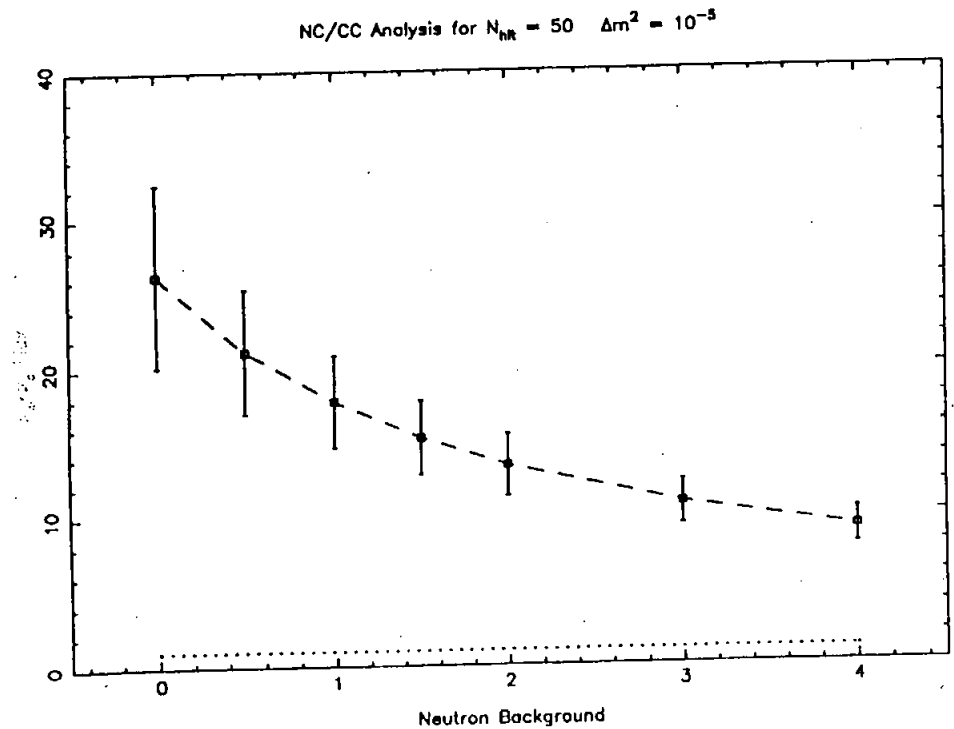
NC/CC Analysis for N_{hlt} = 50 $\Delta m^2 = 10^{-5}$
Neutron Background

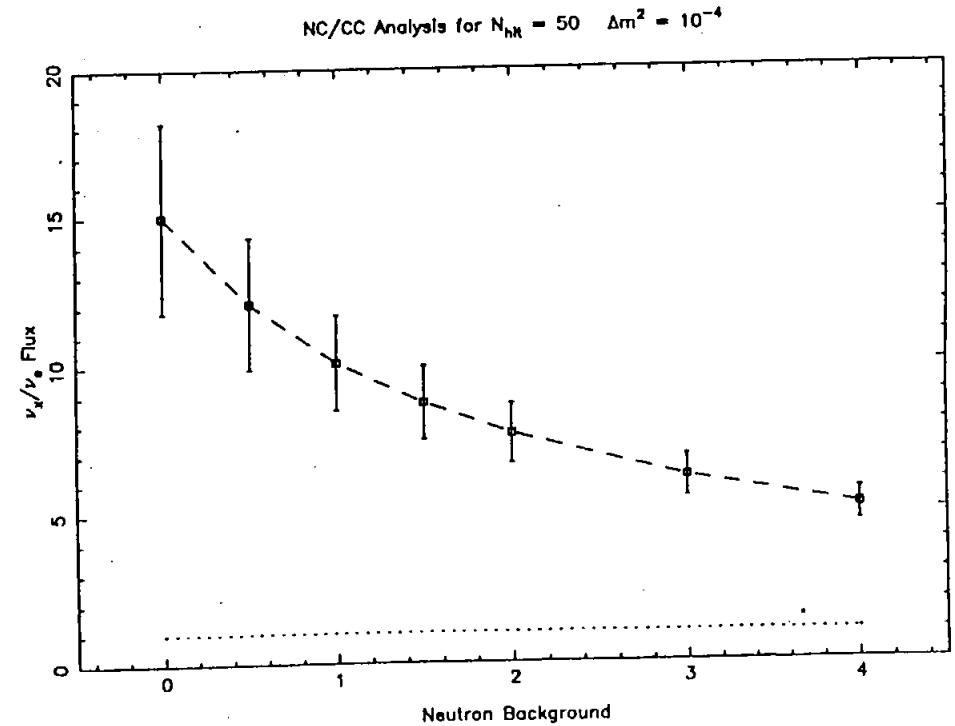
NC/CC Analysis for N_{hlt} = 50 $\Delta m^2 = 10^{-4}$
ν_x/ν_e Flux
Neutron Background

Fig 12

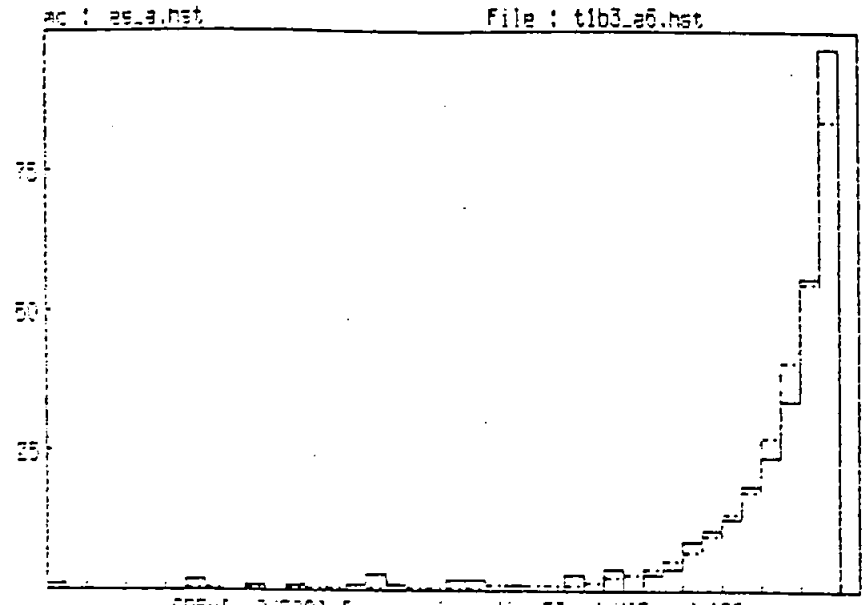

view 1

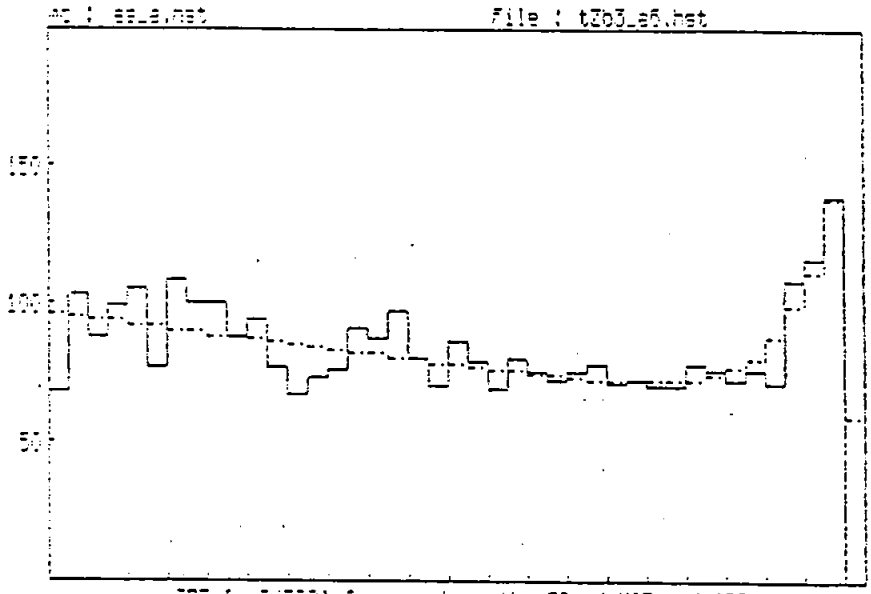

view 2

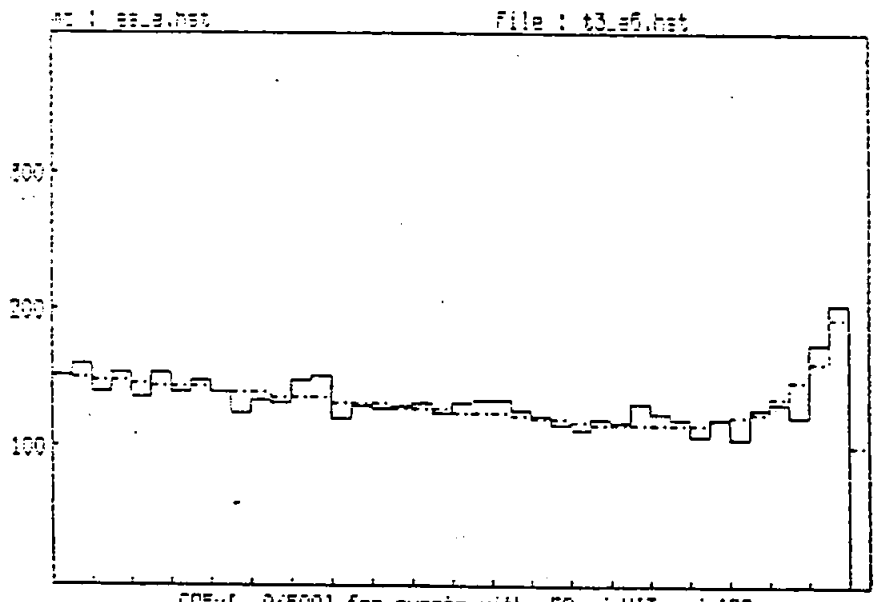

view 3

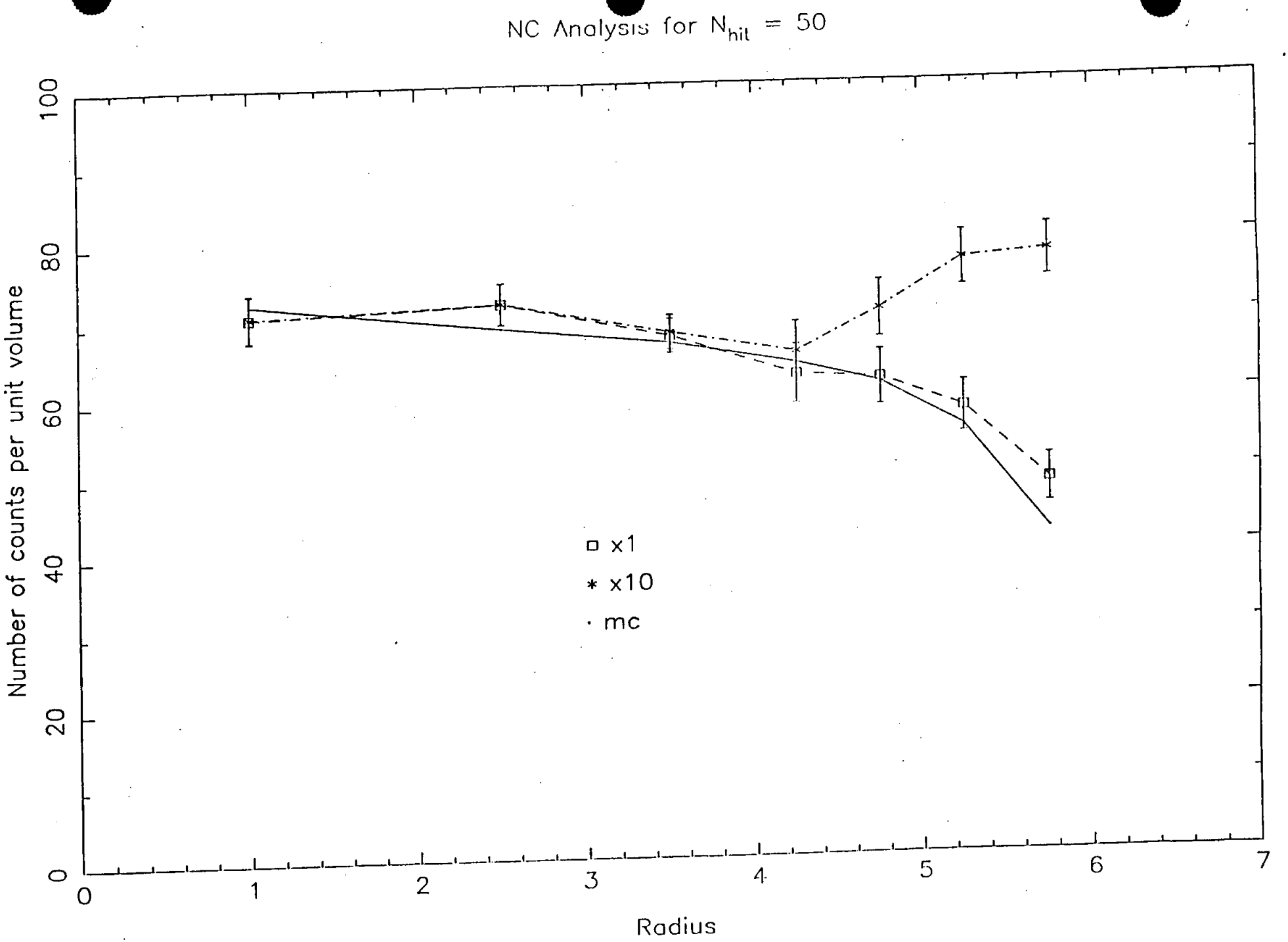
NC Analysis for N_{hit} = 50
Number of counts per unit volume
Radius
0
20
40
60
80
100
0
1
2
3
4
5
6
7
x1
x10
mc

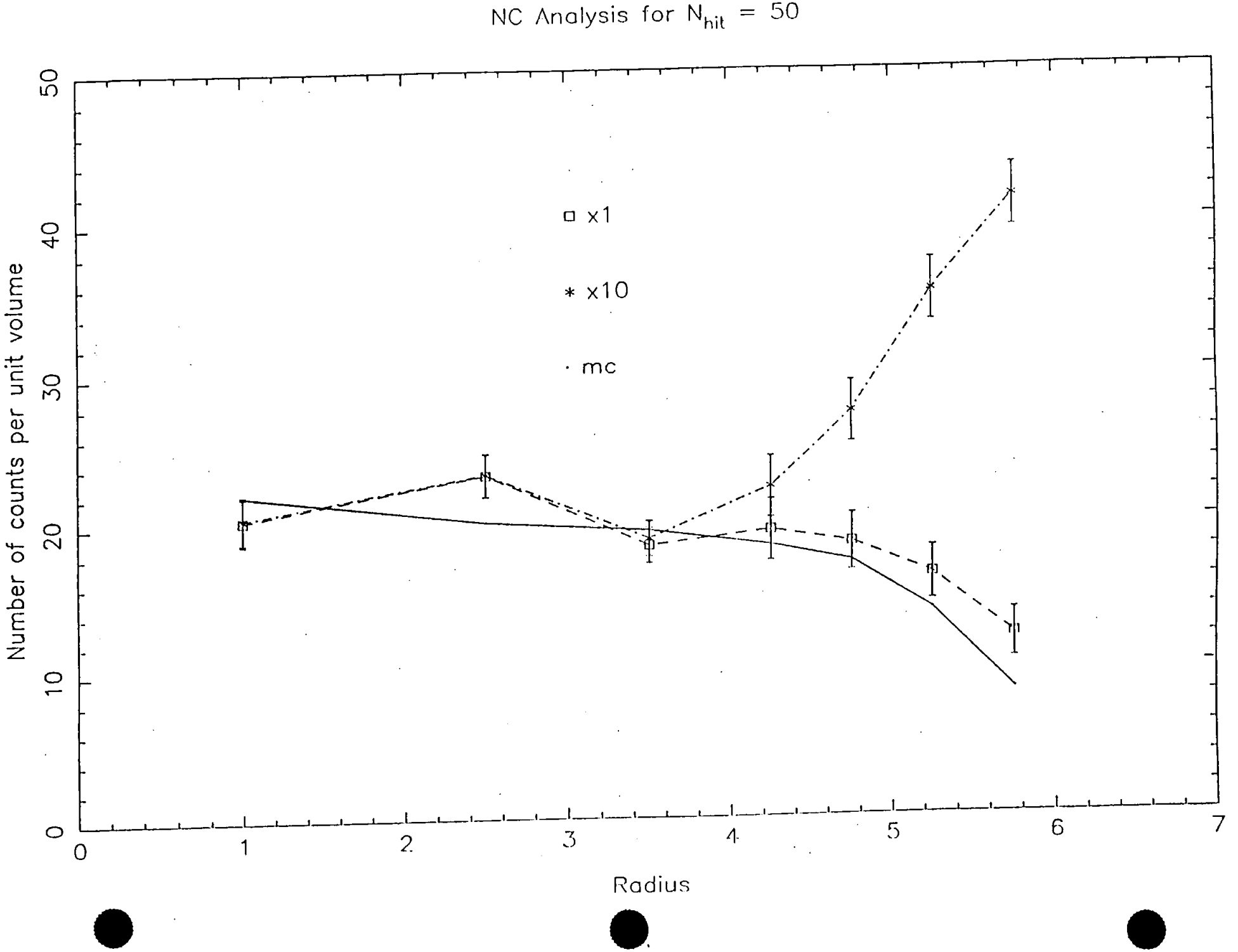
NC Analysis for N_{hit} = 50
Number of counts per unit volume
Radius
x1
x10
mc
0
10
20
30
40
50
0
1
2
3
4
5
6
7

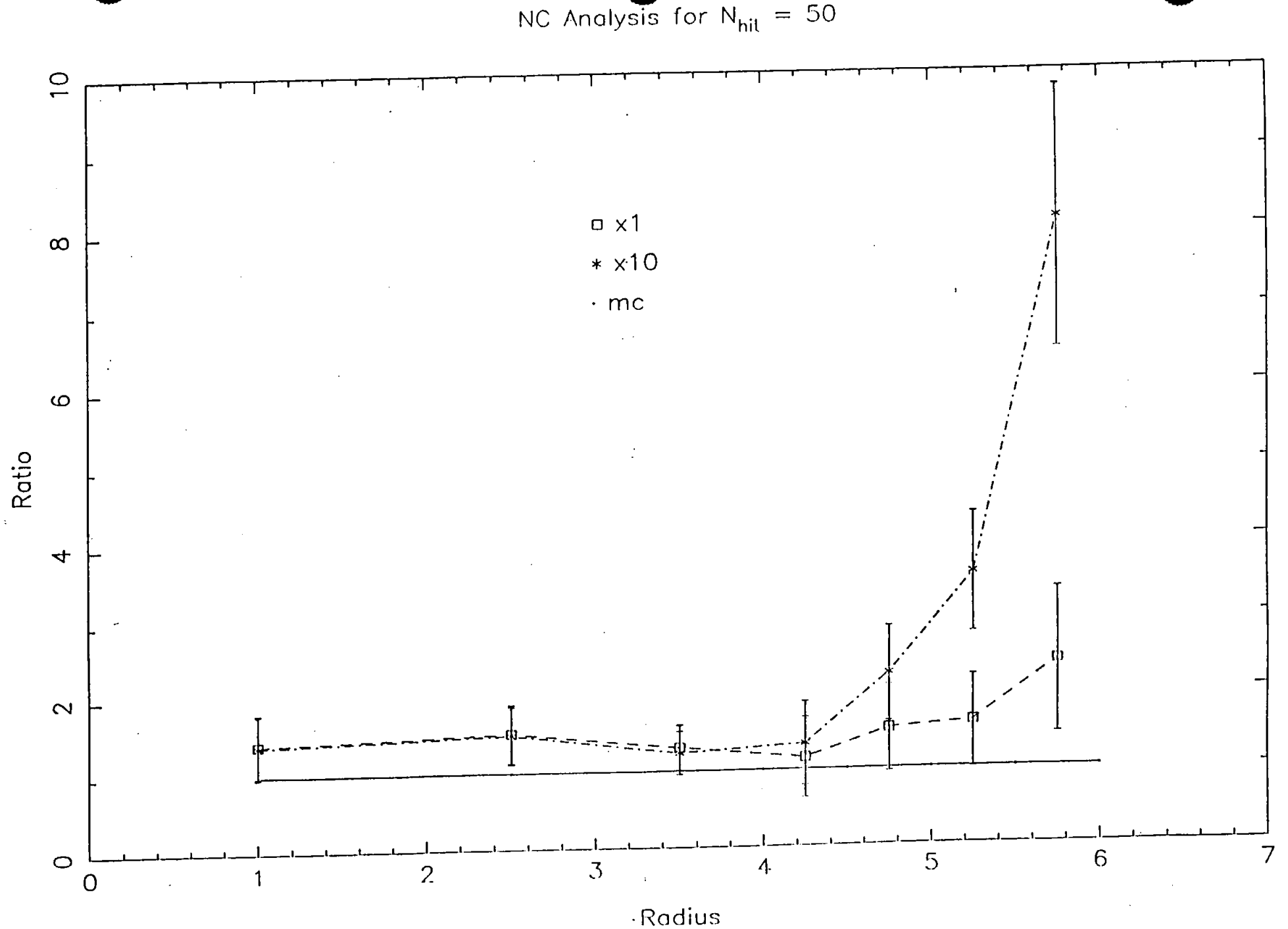
NC Analysis for N_{hit} = 50
x1
x10
mc
Ratio
Radius
0
2
4
6
8
10
0
1
2
3
4
5
6
7

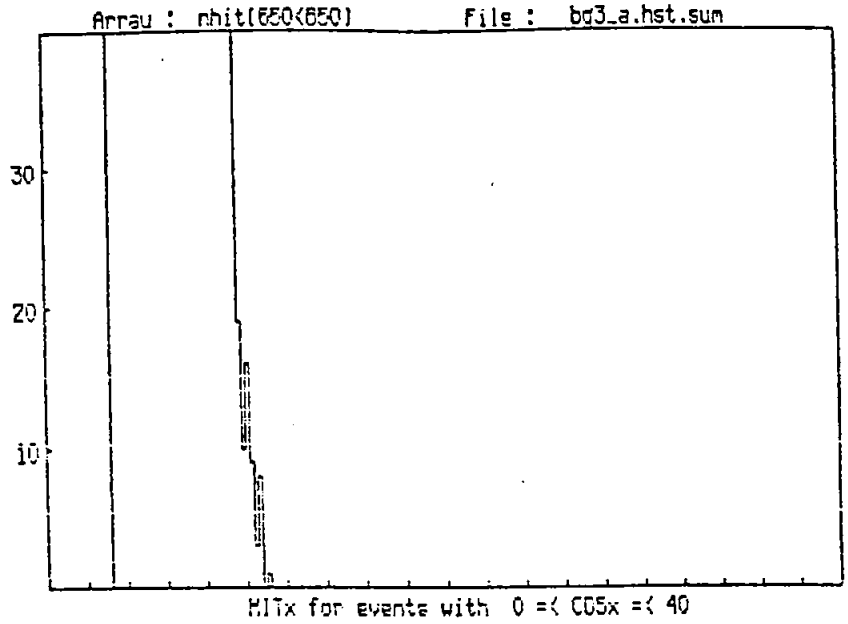

B-γ's.

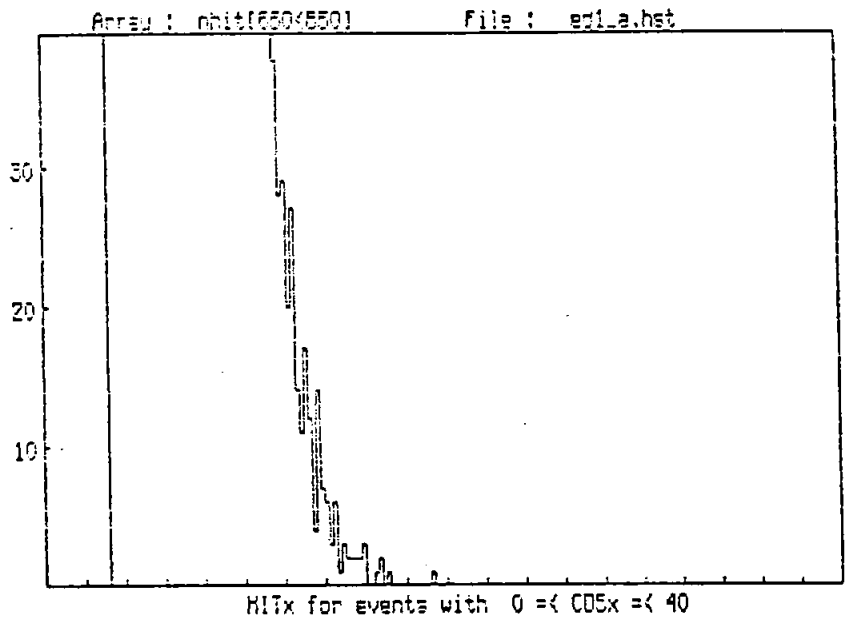

high energy γ's

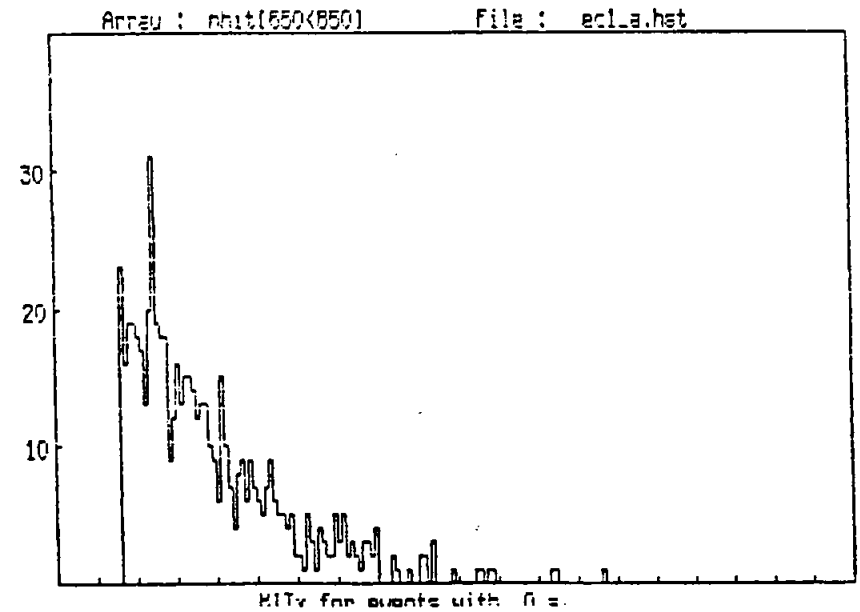

ES

Fig 17

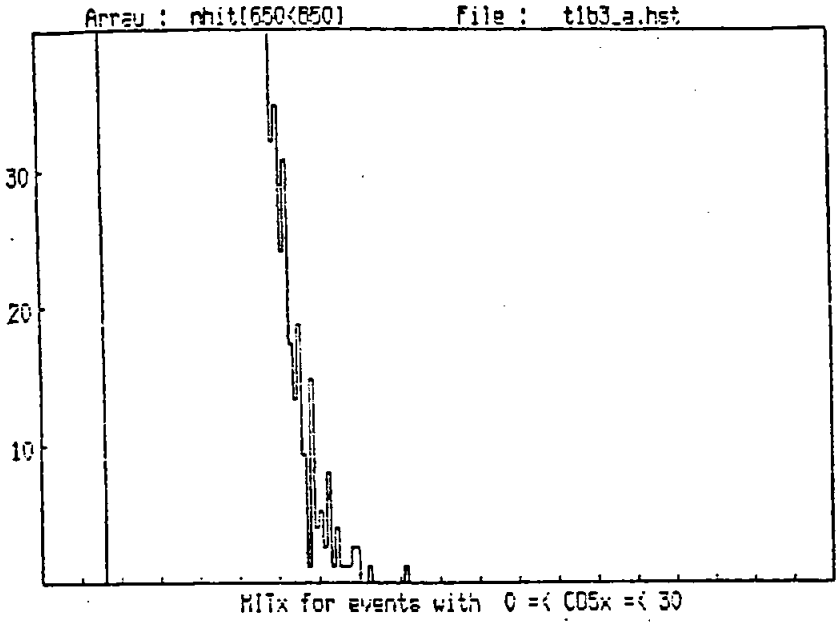

Total

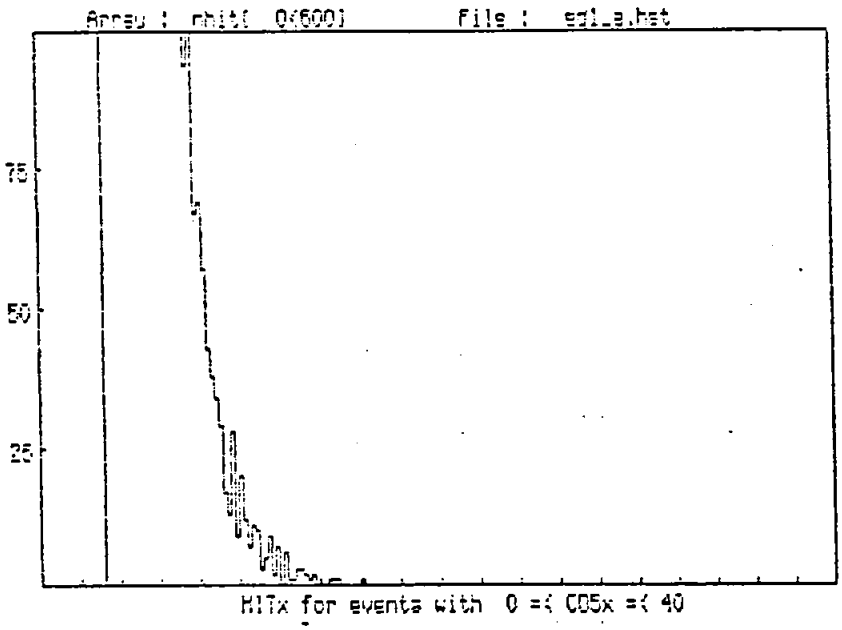

high energy γ's